Interplane coupling and superconducting properties of $Cu_{0.5}Tl_{0.5}Ba_2(Ca_{2-x}Na_x)\ Cu_3O_{10-y}$ (x= 0, 0.25, 0.5, 1) Samples

By Aqsa Bashir

DEPARTMENT OF PHYSICS

Quaid-e-Azam University

Islamabad, Pakistan

2023

Certificate

This is to certify that Ms. Aqsa Bashir D/O Muhammad Bashir has carried out the experimental work in this dissertation under my supervision in the Material Science Laboratory, Department of Physics, Quaid-e-Azam University, Islamabad and satisfying the dissertation requirement for the degree of Master of Philosophy in Physics.

Supervisor

Dr Nawazish Ali

Department of physics

Quaid-e-Azam University

Islamabad, Pakistan

Chairman

Dr Kashif Sabeeh

Department of Physics

Quaid-e-Azam University

Islamabad, Pakistan

Acknowledgements

All the praises to Almighty ALLAH, the most merciful and the sovereign power, who made me able to accomplish this research work successfully. I offer my humble and sincere words of thanks to his Holy Prophet Muhammad (P.B.U.H) who is forever a source of guidance and knowledge for humanity. This work would have not been possible without the invaluable contributions of many individuals. First and foremost, I thank my supervisor **Dr. Nawazish Ali** for all of his support, advice, and guidance during the whole period of my study. I would like to thank to all my junior, seniors and all my lab fellows especially Maria Mushtaq, Hira nazir, Javeria, Mehwish, Sadia, Anila kanwal and co supervisor **Dr. Hamza** for their technical guidance and support. My humble and heartfelt gratitude is reserved for my beloved family specially my brother. Without their prayers, support and encouragement the completion of this study task would have been a dream.

Abstract:

I have synthesized Na doped $Cu_{0.5}Tl_{0.5}Ba_2(Ca_{2-x}Na_x)\ Cu_3O_{10-y}$ (x=0, 0.25, 0.5, 1) samples for the studies of role of lower oxidation state at the inter-planar sites in the mechanism of high T_c superconductivity. The main objective of these studies is to understand the role of oxidation state of atoms at the inter- CuO_2-plane sites in determining the phase coherence of the carriers and its role in the mechanism of high T_c superconductivity. The samples are synthesized by a two-step solid-state reaction method and their superconducting properties are studied by x-ray diffraction analysis, FTIR absorption measurements, resistivity measurements, Fluctuation-Induced Conductivity, and variable Range Hopping model for the semiconducting sample. These samples have shown orthorhombic crystal structure in which their c-axis length increases and the volume of unit cell suppresses with increased Na doping in the final compound. The FTIR absorption measurements of these samples have shown softening of apical oxygen mode of type Cu(1)-O_A-Cu (2) Tl-O_A-CuO_2 and CuO_2 planar oxygen mode in Na-doped samples. $Cu_{0.5}Tl_{0.5}Ba_2(Ca_{2-x}Na_x)\ Cu_3O_{10-y}$ (x=0, 0.25, 0.5) samples have shown metallic variation of resistivity from room temperature down to onset of superconductivity with onset of superconductivity around 102, 100, 98K and zero resistivity critical temperature at 98, 92, 90K, respectively. $Cu_{0.5}Tl_{0.5}Ba_2(Ca_{2-x}Na_x)\ Cu_3O_{10-y}$ (x=1) sample have, however, shown semiconducting behavior that followed the variable range hopping conductivity with energy of activation around 4.2meV. Excess conductivity analyses of $Cu_{0.5}Tl_{0.5}Ba_2(Ca_{2-x}Na_x)\ Cu_3O_{10-y}$ (x=0, 0.25, 0.5) samples have shown the values of coherence length along the c-axis $\xi_c(0)$, the inter-layer coupling J, the Fermi velocity V_F and the phase relaxation time τ_ϕ of the carriers are not significantly altered with Na-doping in the final compound. Moreover, the values of $B_{c0}(T)$, $B_{c1}(T)$, and $J_c(0)$ are not significantly altered in Na-doped samples showing that the population of inadvertent defects acting as the pinning centers are not significantly changed in doped samples. The values of London penetration depth and the Ginzburg-Landau (GL) parameter $\kappa=\lambda/\xi$ in Na-doped samples are, therefore, not significantly changed in Na-doped samples. These studies have demonstrated that the intrinsic superconductivity parameters remain unchanged despite variation in the X-ray diffraction spectra, the softening of phonon modes, and the suppression of the zero-resistivity critical temperature, displayed the importance of phase coherence of the carriers in various CuO_2 planes in the mechanism of high T_c superconductivity. The doped Na-atoms promote the de-coupling of CuO_2

planes that in turn suppress phase coherence of the carriers in the various conducting planes demonstrating importance of it in the mechanism of high T_c superconductivity.

Chapter # 1 Introduction to Superconductivity

Chapter # 2 Literature Review

Chapter # 3 Synthesis and Experimental Techniques

Chapter# 4 Results and Discussions

LIST OF FIGURES

List of tables

Chapter# 1

1.1 HISTORICAL BACKGROUND OF SUPERCONDUCTIVITY:

When a sample, is cooled to a sufficiently low temperature, a phenomenon known as superconductivity occurs in which the electrical resistance of man-made metals and alloys abruptly reduces to zero. Kamerlingh Onnes and his student first noticed it in Leiden in 1911 **[1].** The first metal that shows superconductivity is Mercury (Hg), during the experiment, its critical temperature of 4.2K is observed below which its resistivity goes down to zero.

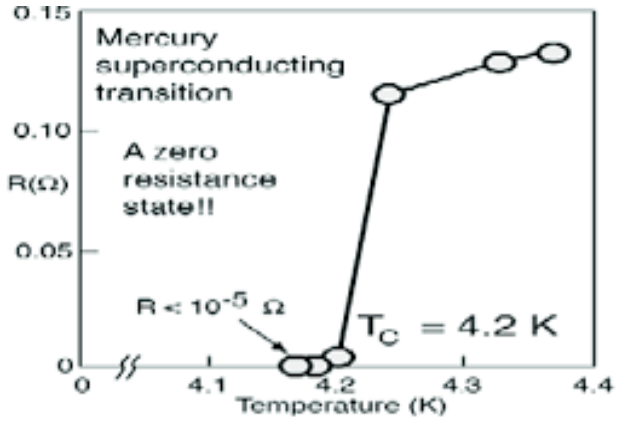

Figure 1.1 Resistivity versus temperature graph of Mercury

Superconductivity occurs in metals, alloys, intermetallic compounds, and doped semiconductors. In 1911 the superconductivity for Hg is observed with T_c=4.2K. In 1973, it was observed for Nb_3Ge with 23K.In 1986, it was observed for $LaBaCuO_4$ with T_c=35K and $YBa_2Cu_3O_7$ with Tc=92K. In 1987, it was observed for $BiCaSrCu_2O_9$ with Tc=110K. In 1988, it was observed for $Tl_xSr_xBa_xCu_xO_x$ with T_c=125K

1.2 SUPERCONDUCTIVITY:

The resistance of various materials and alloys drops to zero, by gradually cooling them at specific temperature. This process is known as superconductivity and the material displaying this property

are called as superconductors **[1].** The critical temperature, abbreviated T_c, is the point in time when the superconductive state changes its state from its normal state to a coherence state.

.

In the process of superconductivity, the state of the superconducting carriers changes to a more ordered state. The same thing happens when the material is placed in the magnetic field and as consequence of applied field system moves from an ordered superconducting phase to a disordered normal material **[2].** Superconductivity is quantum mechanical phenomena and there are two characteristics associated with superconducting state.

I. Perfect diamagnetic

II. Zero electrical resistance

Perfect diamagnetism shown by superconductors is also called Meissner effect and the magnetic field is entirely expelled from the interior of material when it enters a superconducting state.

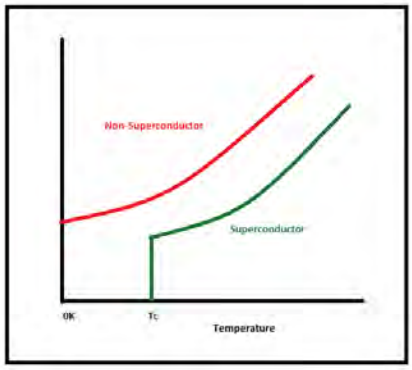

Fig 1.2: resistance-temperature curve for superconductor

The electrical resistivity arises due to lattice vibrations and due to interaction of electrons with atoms. This resistivity vanishes in superconducting state because at lower temperature the system attain lower energy state with the formation of Cooper-pairs. Also, there is no more interaction of electrons with impurities. The superconducting state is also called more ordered state and this order is due to the loose pair of electrons. These electrons form cooper pairs below T_c and also above T_c, they tend to lose their pairing. This ordering of electrons was explained by Bardeen, Cooper and Schrieffer.

1.2.1 Zero Resistivity:

Resistance is the opposition to the flow of electron. In normal state, an electron makes countless collisions with fixed atoms, transfers its energy to the lattice atoms which vibrates and lose energy in the form of heat. As a result, energy keeps on dissipating. The resistivity (ρ) is defined as

$$\sigma = ne^2 \frac{\tau}{m} \quad \text{..... (1.1)}$$

$$\rho = \frac{1}{\sigma}$$

$$\rho = \frac{m}{n\tau e^2} \quad \text{……. (1.2)}$$

Where m is mass of electron, τ is mean free time, e is charge on an electron and n is number density of electrons. By slowly cooling the sample, the density of lattice vibrations starts decreasing and as results the resistivity suppresses. The mean free path of the carriers increases with decrease in temperature. Therefore, for infinite mean free time, the electrical resistivity vanishes completely in superconductors at certain low temperature.

1.2.2 Perfect Diamagnetism:

When we place diamagnetic materials in an external magnetic field, these materials create an induced magnetic field in opposite direction and their magnetic moments align themselves in a manner that they oppose external magnetic field. This phenomenon is known as diamagnetism. **[3]**

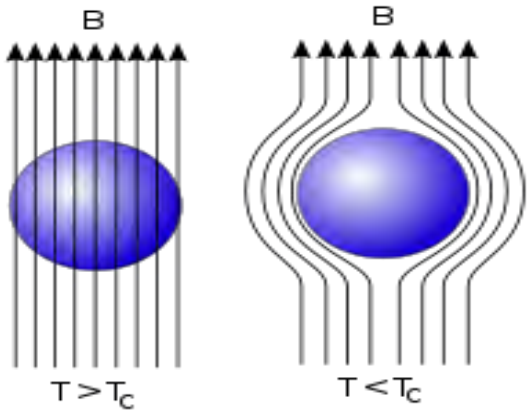

Fig1.3: Meissner's effect in a material

In 1933, Meissner and Ochsenfeld observed that when they placed a superconducting sample in external magnetic field, their sample expelled magnetic flux from the interior of the sample. It's called Meissner's Effect and the superconductor shows diamagnetism response.

Since,

$$B = \mu_o(H + M) \quad \ldots\ldots\ldots\ldots (1.3)$$

As the magnetic field disappears in the superconductor so B = 0

$$0 = \mu_o(H + M)$$

$$M = - H$$

Therefore, the susceptibility is

$$\frac{M}{H} = \chi = -1$$

$$\chi = - 1 \quad \ldots\ldots\ldots\ldots\ldots\ldots (1.4)$$

This is the susceptibility of perfect diamagnetic substance, so superconductors show perfect diamagnetism.

1.3 PARAMETERS OF SUPERCONDUCTING STATE:

The three essential parameters of superconducting state are:

- Critical temperature T_c
- Critical field H_c
- Critical current density J_c

1.3.1 Critical Temperature T_c:

The material's resistance reduces to zero when it becomes superconducting. The temperature at which this happens is called critical temperature. Above critical temperature, reasonable resistivity exists but below this temperature the resistivity completely vanishes. The critical temperature of different superconductors is given below:

Material	Tc
Hg	4.6
Nb	9.26
C6Ca	11.5
Nb3Sn	18.3
$TlSrLaCuO_5$	40
YBCuO	95
TlBa2Ca2Cu3O9	120

Table 1.1 critical temperature of different superconductors

1.3.2 Critical Current Density J_c:

As superconductors have virtually little resistance, thin wires made of them are employed for enormous currents. But still there exists an upper limit to the current flow above which the sample loses its superconducting properties and return to normal state. The maximum current density a superconductor can carry in superconducting state is referred to as critical current density (J_c). J_C was first observed by a scientist named as Kunzler in 1961 **[4].** Critical current density is temperature dependent**.**

1.3.3 Critical Magnetic Field H_c:

Superconductivity is not only destructed by current above its critical value, but it can also be shattered by increasing external magnetic field known as critical magnetic field. This was first observed by Meissner who was studying the superconductor's behaviour at different magnetic field and he stated that after a specific magnetic field value superconductor will shift to normal state. The critical field is temperature dependent when the temperature rises from zero to Tc, critical field gradually decreases. The variation of critical field with temperature is given by following relation:

$$H_c (T) = H_c (0) [1-(T/T_c)]$$

1.3.4 Correlation Between These Three Critical Values:

The three critical values are interdependent. The maximum values of J_c and H_c are observed at zero Kelvin. However, when the temperature reaches its critical value, both J_c and H_c become zero. Plotting these three

critical values results in a critical surface. Inside this critical surface, the material exhibits superconducting behavior, while outside it, the material remains in a normal state.

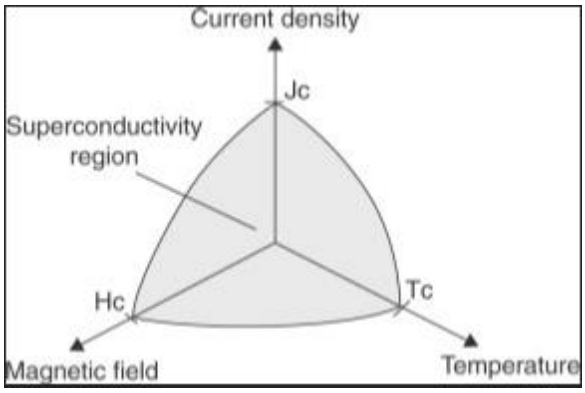

Fig 1.4: critical magnetic field as a function of temperature

1.4 kinds of a Superconductors:

Type I and Type II are the two main categories under which superconductors fall with respect to their exposure to the external magnetic field. Type I superconductors are pure metals, such as lead, mercury, and tin**.** Type II superconductors are alloys or compounds that contain a mixture of metals and non-metals. **[5].** While studying the superconducting alloys in a strong magnetic field the L. Shubnikov experimentally observed the Type II superconductors. According to V. Ginzburg and L. Landau, those with the positive free energy of the normal metallic superconducting interface are Type I superconductors, and those with negative free energy in a strong external magnetic field are Type II superconductors. But at that time only Type I superconductors were known. The theory for Type II superconductors was further refined by A.A. Abrikosov **[6**].

1.4.1 Type-I superconductors:

The definition and characteristics of Type I or soft superconductors are as follows:

a) Type I superconductors are those superconductors that abruptly or quickly lose their superconductivity when exposed to an external magnetic field. The Type I superconductor loses its superconductivity abruptly at the critical magnetic field (H_c), as shown in the figure 1.5.

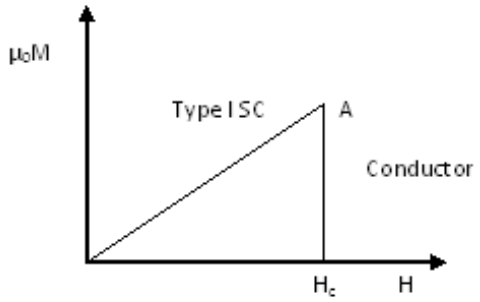

Fig 1.5: Type I Superconductors

b) A conductor will become non-superconducting after reaching the critical magnetic field (Hc) in the Type I superconductor.

c) Because they lose their superconductivity quickly, Type I superconductors are soft superconductors.

d) Type I superconductors perfectly obey the Meissner effect.

1.4.2 Type-II superconductors:

Type II or hard superconductors have the following characteristics:

a)Type II superconductors gradually lose their superconductivity rather than abruptly when exposed to an external magnetic field. The figure 1.6 shows that the Type II superconductor which loses its superconductivity quickly. In the presence of a magnetic field at the lower critical magnetic field (Hc1), Type II superconductors begin to lose their superconductivity, and at the higher critical magnetic field (H_{c2}), they completely lose it.

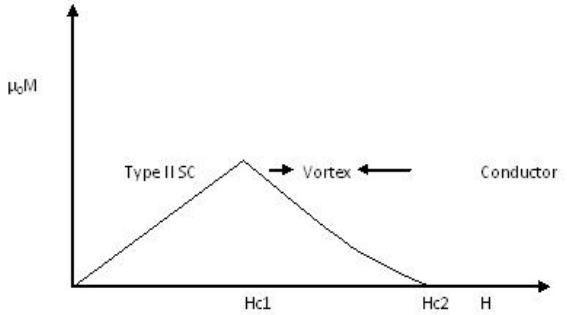

Fig 1.6: Superconductors of Type II

b) The vortex state or intermediate state is the region between H_{c1} and H_{c2}, which stand for the lower and higher critical magnetic fields, respectively.

After H_{c2}, the Type II superconductor will transform into a normal conductor.

c) Type II superconductors are also known as hard superconductors since they gradually lose their superconducting properties rather than abruptly.

d) The Meissner effect is partially obeyed by type-II superconductors.

e) Type II superconductors include NbN (Hc = 8 x 10^6 Tesla) and $BaBi_3$ (H_c = 5.9 x 10^3 Tesla).

f) Utilization of Type II superconductor: Strong field superconducting magnets are a common use for Type II superconductors.

1.5 Evolution of Theory of Superconductivity:

In the wake of superconductivity's discovery, different scientists were working on the theory of superconductivity and many theories were given to explain the phenomenon of superconductivity. In 1935, the two brothers Heinz and Fritz London gave the very first phenomenological theory. Their theory was based on two fluid model. Another theory, which employed the wave function " as an order parameter, was presented by V.L. Ginzburg and L.D. Landau. It was the first quantum theory to explain superconductivity. John Bardeen, Leon Neil Cooper, and John Robert Schrieffer presented the Bardeen-Cooper-Schrrieffer (BCS) theory, the first microscopic theory of superconductivity in 1957.

1.5.1 London theory:

In 1935, two brothers Heinz and Fritz London developed a theory to describe the Meissner's effect. They used two fluid model, they divided all the electrons of superconducting samples into two types; normal electrons "n_n" and superconducting electrons "n_s", so total density is n= $n_s + n_n$. As temperature approaches to critical temperature($T \to Tc$), the number of superconducting electrons would be maximum.

$$T \to Tc, n_n \to 0 \;\; so \;\; n_s \to \max for \; (T<Tc)$$

And $$T \to Tc, n_s \to 0 \; so \; n_n \to \max as \;\; for \; (T>Tc)$$

Consider the uniform electromagnetic field applied on the superconducting sample. As both fields are so weak, we assume that they have no effect on the superconducting electrons. If v_s is the average speed, m is the mass, and e is the super electron's charge, then the equation of motion in the presence of field E is

$$m \, (d \, v_s / d \, t) = -e \, E \quad \ldots\ldots\ldots\ldots\ldots \; \textbf{(1.5)}$$

The current density of superconducting electron is given by

$$J_S = -e\, n_s V_s \quad \ldots\ldots\ldots\ldots\ldots\ldots \textbf{(1.6)}$$

From question 1.5 and 1.6 we have

$$dJ_s/dt = (n_s e^2/m)\, E \quad \ldots\ldots\ldots\ldots\ldots\ldots \textbf{(1.7)}$$

This equation, also referred to as the first London equation, which demonstrates that steady state current J_S is constant in the absence of an electric field. On the other hand, the current density of the normal electrons is $J_n = \sigma E$. Shows that E=0, typical behaviour of normal state.

The Maxwell equation is,

$$\nabla \times E = -\, dB/d\,t \quad \ldots\ldots\ldots\ldots\ldots\ldots \textbf{(1.8)}$$

As E=0 i.e. B = constant within a superconductor. This is not following the Meissner effect so London brothers revised the equation as:

$$\nabla \times J_s = -\frac{n_s e^2}{m} B \quad \ldots\ldots\ldots\ldots\ldots\ldots \textbf{(1.9)}$$

Known as London second equation and result is in agreement with the experiment.

1.5.1.1 London penetration depth:

When we apply magnetic field lines on the superconductor's surface, magnetic field lines can penetrate into the superconductor to the length called London penetration depth denoted as λ_L, which decays exponentially.

Using Maxwell's equation,

$$\nabla \times B = \mu_o J_s \quad \ldots\ldots\ldots\ldots\ldots\ldots \textbf{(1.10)}$$

By taking curl and using equation 1.9,

$$\nabla \times (\nabla \times B) = -\frac{\mu_o n_s e^2}{m} B = -\frac{1}{\lambda^2} B \ldots\ldots\ldots\ldots\ldots\ldots \textbf{(1.11)}$$

where

$$\lambda_L = (m_e/\mu_o n_s e^2)^{1/2}$$

is London penetration depth.

As $$\nabla \times (\nabla \times B) = \nabla (\nabla . B) - \nabla^2 B$$

And as we know

$$(\nabla . B) = 0$$

So, equation 1.10 becomes,

$$\nabla^2 B = \frac{1}{\lambda^2} B$$

For 1-dimension, solution is

$$B = B_o e^{-x/\lambda L} \qquad \text{..... (1.12)}$$

And $\mathbf{B_o}$ is externally applied field and values of λ_L varies from 50nm to 500nm.

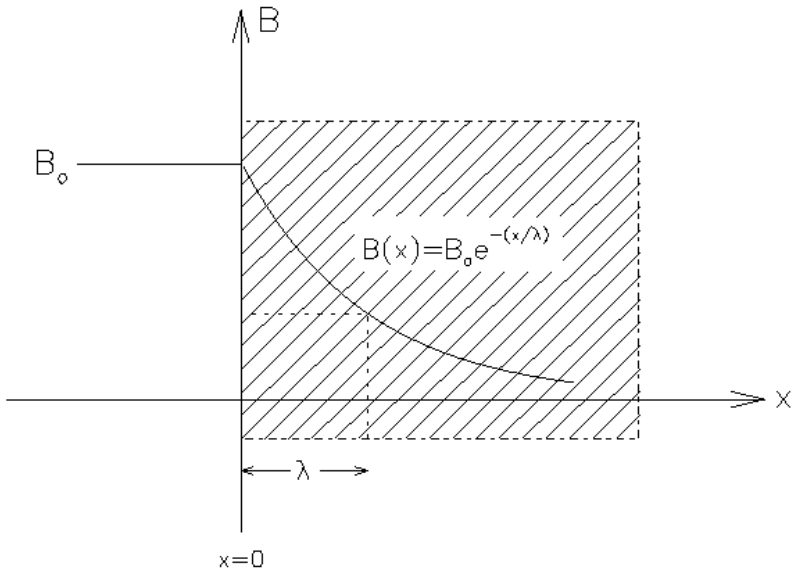

Fig. 1.7: Magnetic field decay within the superconducting substance

London penetration depth also depends on the temperature. The penetration depth decreases with increasing temperature and relation is,

$$\lambda(T) = \frac{\lambda(0)}{[1+(\frac{T}{T_c})^4]^{1/2}} \qquad \text{..... (1.13)}$$

and $\lambda(0)$ is penetration depth at zero Kelvin temperature.

GL theory explained that wave function Ψ should be order parameters of the superconducting electrons. It is a superconductor's macroscopic wave function.

1.5.2. Ginzburg-Landau Theory:

The GL theory, a pioneering quantum theory of superconductivity, was proposed by V.L. Ginzburg and L.D. Landau in 1950. They employed a wave function with the symbol that is dependent on the spatial

coordinate. They asserted that an order parameter exists **[9]** and according to them, Normal state or above the critical temperature T_C have an order parameter of zero. A superconducting condition or a temperature below the critical temperature Tc, i.e.

$$\Psi(T) = 0 \quad ; \text{If} \qquad T > T_c$$

$$\Psi(T) \neq 0 \quad ; \text{If} \qquad T < T_c$$

so basically, it suggests about the state of a system.

GL theory explained that wave function Ψ should be a complex number. It is a superconductor's macroscopic wave function. They weren't very clear about it when they first started working on the meaning of.

1.5.3 BCS theory:

Bardeen, Cooper and Schrieffer proposed first microscopic theory which gave a quantum mechanical explanation of superconductivity in 1957, named as BCS theory **[10]**. This theory is based on advance quantum mechanical concepts. This theory enlightened pairing of two electrons via electron-phonon connection, which is the basis of superconductivity.

1.5.3.1 Formation of Cooper pairs:

According to BCS theory, when electrons pass through the perfectly arranged positive ions, they produce deformation in the crystal lattice.

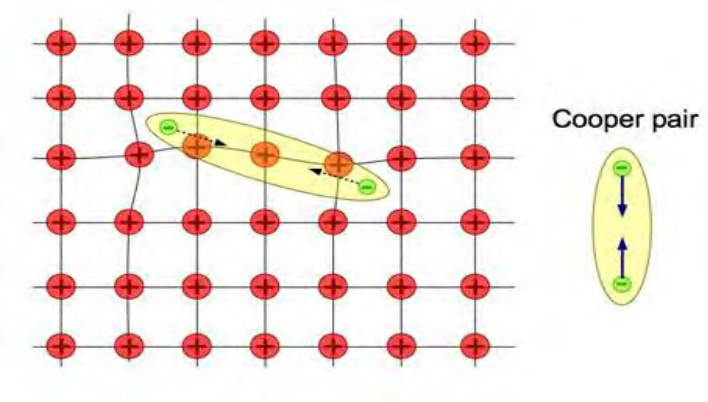

Fig. 1.8: Lattice of a superconductor and formation of Cooper pair.

As a result, atoms of lattice vibrate, producing quanta of lattice vibrations known as phonons. In a metal, an electron moves freely, repelled from other electrons due to same charges but they attract the ions and

this attraction deforms lattice. As ions attracted towards an electron and offer more positive charge to it to form a positive ion core. This greater positively charged ion core attracts other electron of opposite momentum and spin **[11].** As electrons are fermions, but their total spin turns zero like bosons. Many Cooper pairs can be in a same state like bosons. This pair of electrons known as Cooper pair. The Cooper pair is main reason for superconductivity.

1.5.3.2 Coherence Length (ξ):

In cooper pair, electrons are not necessarily close, they may be far apart because their interaction has long range, may be of few hundred nanometers. There is some distance between them **[12]** and this distance between them is known as coherence length (ξ). In high temperature superconductors, coherence length is small and in case of low temperature superconductors value of coherence length is large. According to BCS theory, the coherence length is,

$$\xi = \frac{\hbar V_F}{2\Delta}$$

Where V_F is he Fermi Velocity and 2Δ is the energy gap.

For type I superconductors: $\xi > \lambda_L$

For type II superconductors: $\xi < \lambda_L$

1.6 Isotope Effect:

In 1950, H. Froehlich **[13]** suggested lattice vibration is essential in causing the materials to superconduct. He proposed that whether incorporation of neutrons in the nucleus (i.e. changing the isotope of any element doped in the superconductor) affect these vibrations or not? Later this year, Maxwell and C.A. Reynolds found isotope effect in superconductors. Isotope effect says that the temperature of superconductor transition varies inversely with mass of isotope. The mathematical form of the isotope effect is

$$T_C \propto M^{-\alpha}$$

Or $$M^{\alpha}T_c = \text{constant} \ldots\ldots$$

1.7 Josephson Effect:

Quantum mechanical tunneling effect in superconductors was first projected by B.D. Josephson in 1962 **[14]**. He sandwiched a thin insulating layer between two superconductors to make Josephson junction. The insulating layer should be thin enough, of the order of 10 nm, so that Cooper-pairs can tunnel under the obstruction.

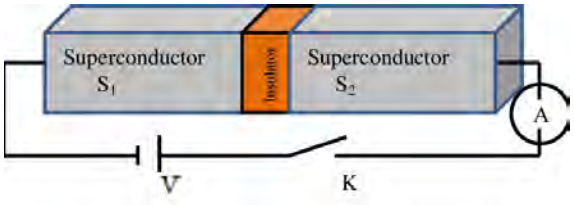

Fig 1.9: Josephson junction

Josephson Effect is categorized into two kinds:

- DC Josephson Effect

- AC Josephson Effect

1.7.1 DC Josephson Effect:

In 1962, Josephson determined the current which was anticipated to flow across the insulating barrier, a cooper pair can tunnel the barrier even in the absence of applied voltage. He found that along with normal current (current produced by the tunneling of unpaired electrons), super-current (current arose due to tunneling of Cooper pairs) also flowed at zero bias. The flow of super-current at zero bias is called the DC Josephson Effect.

1.7.2 AC Josephson Effect:

In the presence of applied external voltage electromagnetic waves are emitted across the junction known as ac-Josephson effect. An alternating super-current begins to flow across the barrier in addition to normal DC

that flows due to tunneling of single-electron **[15].** The angular frequency associated radiations across the junction is ω=2eV/$\hbar$. The occurrence of this oscillating current due to Cooper-pair tunneling is called AC Josephson Effect.

1.8 Magnetic Flux Quantization:

In 1961, it was revealed that magnetic flux quantization exists. The scientists in Germany and USA separately discovered it at almost same time [16]. To understand the term flux quantization, first consider a superconducting loop, initially at temperature $T > T_c$, and is exposed to a magnetic field from the outside. When the temperature of this loop is dropped such that, it falls below critical temperature, then the field lines are pushed out of the material pertaining to Meisner effect. Meanwhile, the flux trapped in the loop remains there and it stays there even if the external field is removed. It happens when the external field is no longer there, the magnetic flux through the loop first decreases, then due to Faradays law of induction, current is induced in the loop, but as now the loop is in superconducting state, the currents continue to flow without losses, and it starts to support the flux. If the ring had some resistance, the current would have decreased and the flux would also have decayed, but in this case, flux takes infinite time to decay, thus appeared to be trapped in a loop.

The magnetic field multiplied by the loop's surface area is the definition of magnetic flux. i.e., $\mathbf{\Phi} = \mathbf{B} \cdot \mathbf{A}$. Here $\mathbf{\Phi}$ can have any value but when we talk about superconducting loop then the flux passing through that loop is always quantized. It means that the flux can only attain certain values. The equation for this term is:

$$\Phi = \frac{2ne}{e^*} \Phi_0$$

Where Φ is total flux trapped in a hole and Φ_0 is flux quantum having value $\Phi_0 = 2.07X10^{-7}$ G cm^{2}and e^*=2e (corresponding to cooper pair).

High temperature superconductors: Those superconducting materials with critical temperature more than 23.2K is identified as High Tc superconductors The two scientists provide great superconductive evidence in a new class of superconducting elements in LaBaCuO ceramic at the Tc of 30K. This marvelous discovery has increased the interest towards superconductivity phenomenon. Then in 1987, “P. W. Chu and M. K. Wu”, both of them declared together a disclosure of a 93K superconductor Y-Ba-Cu-O (replacing La by Y). Just after one year in 1988, superconducting cuprates of Bi and Tl based having critical temperatures 110K and 125K respectively were discovered. Then in 1993, Hg-based cuprates having T_c=135K were discovered and their critical temperature increased to 164K. In 1989, one family of doping

of free electrons in cuprates are discovered. Its name was (Nd, Pr and Sm)-Ce-Cu-O. Their maximum critical temperature is T_c=24K. We have used the unconventional high-temperature superconductors which have tetra/orthorhombic perovskite crystal structure having p4m space group. They are highly anisotropic.

1.9 Applications of superconductivity:

In this era, superconducting materials are used mostly in industries and in many research works. Some applications of superconductors, due to their properties, are listed below;

- Magnetic shielding
- Magneto cardiogram
- NMR ("nuclear magnetic resonance spectroscopy")
- Magnetic levitation trains
- Logic elements of superconductors
- Very fast computers
- MRI ("magnetic resonance imaging")
- Non-destructive computer chips
- Mineral prospecting

References:

[1] R. Simon and A. Smith, Superconductors: Conquering Technology's New Frontier, Plenum, New York, (1988).

[2] I.A.C Rose and E.H. Rhoderick, Introduction to Superconductivity, Pergamon Press, (1969).

[3] Solid state physics and Electronics R.K Puri and V.K Babbar, 278(1997)

[4] J. E. Kunzler, E. Buehler, F. S. L. Hsu and J. H. Wernick: Physical Review Letters 6 (3), (1961) 89-91

[5] B.D. Josephson, Phys. Lett. 1 (1962) 251–253.

[6] M.K. Wu, J.R. Ashburn, C.J. Torng, P.H. Hor, R.L. Meng, L. Gao, Z.J. Huang, Y.Q. Wang, C.W. Chu, Phys. Rev. Lett. 58 (1987) 908–910

[7]. F. London, H. London: Proc. Roy. Soc A149, 71

[8]. V. V. Smith book

[9]. P. Mandal, A.Poddar, A.N. Das, B.Ghosh, P.Choudhary: Physica C, 169 (1990) 43-49.

[10]. J. Bardeen, L. N. Cooper and J. R. Schrieffer: Physical Review ,106 (1), (1957) 162-164.

[11]. H. Ibach and H. Lüth, Solid-State Physics: An Introduction to Principles of Materials Science (2009).

[12]. S.O.Pillai, Solid State Physics, 5th Edition, New Age International (p) Limited Publishers (2002).

[13]B.D. Josephson, Phys. Lett. 1 (1962) 251–253.

[14] B.D. Josephson, 'Possible new effects in superconductive tunneling", Physics Letters 1, 251 (1962).

[15] B.D. Josephson, 'The discovery of tunneling supercurrents", Rev. Mod. Phys 46(2), 251-254 (1974)

[16] B.S. Deaver and W.M. Fairbank, Physical Review Letters 7(2), 43 (1961)

Chapter# 2

Literature Review

2.1 Thallium Based Superconductors:

Parkin et al. **[1]** in $Tl_2Ba_2Ca_2Cu_3O_x$ superconductor, got zero resistance critical temperature ranges between 118 and 127 K. They discovered that T_c(R=0) varies with respect to the environment. The $Tl_2Ba_2Ca_2Cu_3O_x$ superconductor has a body-centered tetragonal configuration.

K. Gopala Krishnan et al. **[2]** prepared the Tl-Ba-Ca-Cu-O superconductor and found its zero resistance for T_c(R=0) of 125K. They found it stable and reproducible. XRD analysis shows that the c-axis decreases with decreasing the temperature from 300K to T_c(R=0). They also described the anisotropic thermopower of $Tl_2Ba_2CaCu_2O_8$ single crystals.

Z. Z. Sheng et al. **[3]** discovered thallium-based superconductors for the first time in 1988. They investigated a new Tl-Ba-Ca-Cu-O (TBCCO) compound with T_c of above 100K. They reported that thallium-based superconductor $Tl_2Ca_2Ba_2Cu_3O_{10+y}$ has been shown to exhibit very stable phase with high critical temperatures.

2.2 CuTl-Based High Temperature Superconductors:

$Cu_{0.5}Tl_{0.5}Ba_2Ca_2Cu_{3y}Zn_yO_{10}$, (y=0.75,1.5, 2.25, 2.65) was synthesized by Nawazish A. Khan et al by solid-state reaction method **[4].** According to these authors the XRD of this compound has shown a tetragonal crystal structure. As the zinc doping concentration at the copper site increases, their T_c(R=0) was 121K and T_c(onset) was 127K. The magnitude of the diamagnetism and the T_c(R=0) are both increased.

To enhance interplane coupling, Nawazish A. Khan et al. **[5]** prepared the (CuTl1223) $Cu_{0.5}Tl_{0.5}Ba_2Ca_2Cu_3O_{10-y}$ superconductor with Mg-doping at the calcium-site. They claimed that while the a-axes and c-axes are reduced, the $T_c(R=0)$ and $[J_c(H=0)]$ increased by 10K and 2 orders of magnitude, respectively. The primary crystal phase of $Cu_{1-x}Tl_xBa_2Ca_{2-y}Mg_yCu_3O_{10}$, (y=0, 0.5, 1.0, and 1.5) was discovered through X-ray diffraction.

In order to improve the interplanar coupling Nawazish A. Khan et al. **[6]** synthesized the superconductor $Cu_{0.5}Tl_{0.5}Ba_2Ca_{2y}M_yCu_3O_{10}$, (M = Mg, Pr). The superconducting properties of this compound is demonstrated by experimental results from XRD, Fourier transform Infrared spectroscopy, Four Probe resistivity method, and FIC analysis. They discovered that the apical oxygen mode was softened and the c-axis was reduced. The $T_c(R=0)$ and $J_c(H=0)$ were enhanced by the Mg-doping in the pure sample. But when Pr was doped to a pure 1223 sample then there was decreased behavior of coupling constant 'J'. FTIR results show the hardening of mode Cu (1)–O_A–Cu (2) from 534cm^{-1} to 564 cm^{-1} while the other apical mode of oxygen Tl–O_A–Cu (2) is softened from 485 cm^{-1} to 436 cm^{-1} with increased doping of Pr-concentration.

In order to improve the interplane coupling, Nawazish A. Khan et al. **[7]** added Be at the Calcium-sites in $Cu_{0.5}Tl_{0.5}Ba_2Ca_{n1y}Be_yCu_nO_{2n+4}$ samples. $Cu_{0.5}Tl_{0.5}Ba_2Ca_{2y}Be_yCu_3O_{2n+4}$ (y: 0.7,1.7) and $Cu_{0.5}Tl_{0.5}Ba_2Ca_{3y}Be_yCu_4O_{12}$ samples were synthesized by a two steps solid-state reaction approach. The zero-resistance transition temperature $T_c(R=0)$ was given as 95K. The crystal structure was determined to be tetragonal using X-ray diffraction (XRD). Be-doping was used to lower the cell parameters such as c-axes. The planar oxygen modes observed in the wavenumber of 575 cm^{-1} and the apical oxygen absorption mode around wavenumber 500 cm^{-1} are softened with increased Be-doping. They have also shown that superconductivity volume fraction increases along with increase of inter-plane coupling. The magnitude of diamagnetism as well as the critical temperature $T_c(R=0)$ was found to increase with increased Be-doping in the final compound.

2.3 Literature about FIC analysis:

S. Firdous. et al **[8]** studied the intrinsic parameters of superconductivity on the basis of analysis of excess conductivity for the samples of -$YBa_2Cu_3O_{7-\delta}$, -$YBa_2Cu_4O_8$,& ($Y_2Ba_4Cu_7O_{15-\delta}$). These $Cu_2(CN)_2$ prepared samples have shown superior values of Fermi velocity of the carriers v_F, the c-axis oriented coherence length ξ_c and critical current density J_c in comparison with such samples prepared by using CuO as starting copper compound. However, the CuO synthesized $YBa_2Cu_3O_{7-\delta}$ samples have shown superior infield characteristics showing higher population of inadvertent

defects acting as pinning centers in such samples. The $B_{c0}(T)$ superiority trend for device fabrication have been found in these studies is $YBa_2Cu_3O_{7-\delta}$ > $YBa_2Cu_4O_8$ > $Y_2Ba_4Cu_7O_{15-\delta}$, respectively.

Nawazish Ali Khan **[9]** using two-step solid-state reactions synthesized $Cu_{0.5}Tl_{0.5}Ba_2Ca_2Cu_3O_{10-\delta}$ and $Cu_{0.5}Tl_{0.5}Ba_2Ca_2Cu_{1.5}M_{1.5}O_{10-\delta}$ samples (M = Cd, Zn, and Ni). These samples have an orthorhombic crystal structure in which the addition of M atoms increases the size of the unit cell. $Cu_{0.5}Tl_{0.5}Ba_2Ca_2Cu3O_{10-\delta}$ (M = Cd, Zn, and Ni) $Cu_{0.5}Tl_{0.5}Ba_2Ca_2Cu_{1.5}M_{1.5}O_{10-\delta}$ samples have shown onset of superconductivity around 105.6, 101.7, 114, 106.3K and zero resistivity critical temperatures at 98.3, 95.4, 102.3,102K, respectively. In these samples, the beginning of diamagnetism is observed at various temperatures of 113.6, 105, 105.2, and 107.7 K. The excess conductivity analysis of such samples have shown that coupling between layers of J, Fermi velocity of carriers v_F , coherence length along the $\xi_c(0)$ are suppressed in all doped samples.

Fluctuation Induced Conductivity analysis (FIC) of $Cu_{0.5}Tl_{0.5}Ba_2Ca_{n1}Cu_nO_{2n+4}$ (n = 2, 3, 4) thin film samples were carried out by Nawazish A. Khan et al **[10]**. The c-axis length in such samples increases with increase in number of CuO_2 planes. In such analyses the Ginzburg-Landau and Aslamazov-Larkin theories were employed. With more number of CuO_2 planes present in these samples, the coupling constant J of the CuO_2 conducting planes decreases even though the values of $\xi_c(0)$, v_F are enhanced. However, the values of $B_c(T)$, $B_{c1}(T)$, values, and $J_c(0)$ increase. With increase in number of superconducting planes in $Cu_{0.5}Tl_{0.}5Ba2Can1Cu_nO_{2n+4}$ (n = 2, 3, 4) increases. The value of the London penetration depth suppresses with increase in number of CuO_2 planes.

Nawazish. A. **[11]** used the solid-state reaction technique to synthesize the single phase of $(Tl_{1-y}C_y)Ba_2Ca_3Cu_4O_{12-\delta}$; (y=0, 0.25, 0.5, 0.75) superconductors. The presence of carbon in $(Tl_{1-y}C_y)Ba_2O_{4-\delta}$ charge reservoir layer controls the flow of carriers to the conducting CuO_2 planes. Intrinsic doping of carbon at the thallium site has been validated by FTIR absorption studies. The analysis of grain boundaries of the $Tl_{0.75}C_{0.25}$ -1234 sample has shown improvement in the grain boundaries, as evidenced by the SEM (scanning electron microscope) analysis. In order to attain a large' T_c [R=0] and enhanced grain's shape, it was discovered that carbon doping of y=0.25 was the ideal concentration for better superconducting properties in such compounds. However, in all of the carbon-replaced samples, the degree of diamagnetism has been reduced. Main reason for the suppression of diamagnetism is decrease in the density of pinning centers in such compounds which is mostly filled by doped carbon atoms.

Bulk $(Cu_{0.5}Tl_{0.5})Ba_2Ca_2Cu_3O_x$ superconductor was synthesized using a straightforward solid-state chemical technique by Nawazish Ali Khan **[12]**. They ground Cu(CN), $Ba(NO_3)_2$ and $CaCO_3$ materials by using of mortar and pestle following the firing at 840℃. After firing, Tl_2O_3 was mixed with sample to formed pellets. These pellets enclosed in aluminum foil and heated for 30 min after post-annealing in a nitrogen environment, they used a four-probe resistivity measurement method to find onset T_c at 110 K and T_c(R=0) at 103 K. The FTIR absorption measurement confirmed the formation of material with optimum oxygen doping.

$Cu_{0.5}Tl_{0.5}Ba_2(CaMg)Cu_3O_{10-d}$ and $Cu_{0.5}Tl_{0.5}Ba_2(CaMg)Cu_{1.5}M_{1.5}O_{10-d}$ (M: Zn, Ni)-doped samples were compared in terms of their superconducting properties by S.H. Safeer et al. **[13].** The primary objectives for such studies were to comprehend how electron-phonon interactions affect the high-temperature superconductivity mechanism in these oxide superconductors. In their studies, it was observed that doping Zn and Ni at CuO2 planar sites leads to an-harmonic oscillations that suppress the critical temperature of the final compound. When Zn and Ni atoms were added to the pure compound, the magnitude of diamagnetism was reduced in both the field-cooled (FC) and zero-field-cooled (ZFC) states. Zn and Ni doping suppress the critical current density and width of magnetic hysteresis loops. The population of phonons, which is a crucial requirement for the process of interactions between electrons and phonons, is reduced in the doped samples due to the enhanced an-harmonic oscillations.

$Cu_{0.5}Tl_{0.5}Ba_2Ca_2Cu_{3y}M_yO_{10}$ (M = 0, Si, Ge, Sn, y = 0, 1) samples were synthesized by Nawazish A. Khan et al and investigated their superconducting properties by resistivity, XRD and FTIR absorption measurements **[14]**. These samples followed P4/mmm space group and tetragonal structure. Si doping results in a decrease in the cell parameters, whereas doping of Ge and Sn results in an increase in the values of cell parameters. The magnitude of the superconductivity parameters, namely the magnitude of diamagnetism, T_c(onset) and T_c(R = 0) decrease in Si and Sn doped samples; in contrast, it increases in Ge doped samples.

2.4 Metals-doped 1223 superconductors:

Nawazish.Ali. Khan **[15]** Two-step solid-state reactions were used to prepare $Cu_{0.5}Tl_{0.5}Ba_2(Ca_{2-x}Be_x)$ (Cu_2Ti) O_{10-y} (x=0, 0.5, and 1.0) samples. After adding the concentration of Be at Calcium site of above given compound, superconducting properties were reduced. According to the atomic masses of Titanium (47.90 a.m. u) and Copper (63.54 a.m.u) in conducting CuO2 plane, oxygen phonon modes varied following Be doping. The decrease value of Cooper pairs' density (arise due

to an-harmonic oscillations), below a required level of optimum superconductivity, responsible for the loss in microscopic superconducting parameters that was deduced from the analysis of excess charge carrier conductivity

Doping of CuO_2 planes with Na atoms in the $Cu_{0.5}Tl_{0.5}Ba_2Ca_2Cu_3O_{10-y}$ superconductor is studied for the first time by Nawazish A. Khan **[16].** With doping of Sodium, the magnitude of diamagnetism and the critical temperature T_c[R=0] for zero resistance are both enhanced. However, these superconducting properties are suppressed when doped with Magnesium and Beryllium at the Ca sites. By X-ray diffraction analysis studies of such compounds it was observed that c-axes length is suppressed with Magnesium and Beryllium doping. Na-doped samples self-doped by post-annealing of samples displayed improved superconducting parameters that most likely arise from optimization of carriers in the conducting CuO_2 planes.

R. Awad et al. **[17]** prepared $TlBa_2Ca_{2-x}Na_xCu_3O_{9-\delta}$ with $0 \leq x \leq 0.4$. As the Na content increases, the lattice parameters expand. When x increases from 0 to 0.05, Tc is observed to slightly rise before gradually decreasing for x values greater than 0.05. This observation was explained by the evidence that Na shifted the (Tl-1223) phase from an over doped regime to an underdoped regime, which is in line with the thermopower data indicating a transition from an over doped to an underdoped regime. Additionally, AC magnetic susceptibility experiments have reported the inter-grain critical current density (J_c) as a function of Na.

T. Aytug et al**. [18]** observed both Na-doped and undoped Hg-1223 phases during low-temperature oxygen annealing. It is suggested that by adjusting the oxygen content of the Hg-O layer, Na may disrupt the material's electronic band structure, potentially affecting the superconductivity of the material post-annealing. It has been found that annealing at 300 °C for 10 hours can increase T_c by more than 20 K, but annealing at temperatures above 350 °C leads to a loss of superconductivity due to Hg loss. As the annealing temperatures increase up to 400°C, the normal state begins to diminish. Furthermore, the normal state curves of the doped samples became flatter, indicating a more insulating characteristic.

References:

[1] S. S. P. Parkin et al., "*Bulk Superconductivity at 125 K in $Tl_2Ca_2Ba_2Cu_3O_x$*" Ten Years of Superconductivity: 1980–1990, pp. 309–312, 1988, doi: 10.1007/978-94-011-1622-0_44

[2] K. Gopala Krishnan, P. V. P. S. S. Sastry, K. Gangadharan, G. M. Phatak, J. V. Yakhmi, and R. M. Iyer, "*Synthesis and properties of a 125 K superconductor in the Tl-Ca-Ba-Cu-O system*," Applied Physics Letters, vol. 53, no. 5, pp. 414–416, Aug. 1988, doi: 10.1063/1.100606.

[3] Z. Z. Sheng and A. M. Hermann, "*Bulk superconductivity at 120 K in the Tl–Ca/Ba–Cu–O system,*" Nature, vol. 332, no. 6160, pp. 138–139, Mar. 1988, doi: 10.1038/332138a0.

[4] N. A. Khan and M. Mumtaz, "*A new $Cu_{0.5}Tl_{0.5}Ba_2Ca_2Cu_{3-y}ZnyO_{10-\delta}$high-temperature superconductor with three ZnO2planes*," Superconductor Science and Technology, vol. 19, no. 8, pp. 762–766, Jun. 2006, doi: 10.1088/0953-2048/19/8/012.

[5] N. A. Khan and A. A. Khurram, "*Enhanced superconducting properties of $Cu_{1-x}Tl_xBa_2Ca_{2-y}Mg_yCu_3O_{10-\delta}$ (y=0, 0.5, 1.0, and 1.5*)," Applied Physics Letters, vol. 86, no. 15, p. 152502, Apr. 2005, doi: 10.1063/1.1899254.

[6] N. A Khan, A. Javaid, A. Khurram, and N. Haider, "*The study of inter-plane coupling in $Cu_{0.5}Tl_{0.5}Ba_2Ca_2Cu_3O_{10-\delta}$ superconductor by Mg and Pr substitution at Ca site*," scholar.google.com.pk, Sep. 15, 2006.

[7] N. A Khan, G. Husnain, and K. Sabeeh, "*Superconductivity in Be substituted by Ca in $Cu_{0.5}Tl_{0.5}Ba_2Ca_{n-1-y}Be_yCu_nO_{2n+4-\delta}$ (n= 3, 4 and y= 0.7, 1.5, 1.7, 2.0*)," scholar.google.com.pk, Apr. 01, 2006.

[8] S. F. Akhtar, N. A. Khan, and S. H. Safeer, *"Excess Conductivity Analysis of Y-Ba-Cu–O Superconductor Phases,*" Journal of Low-Temperature Physics, vol. 206, no. 1, pp. 106–119, Jan. 2022, doi: 10.1007/s10909-021-02629-0

[9] Abu Aly, A.I., Ibrahim, I.H., Awad, R.A., El-Harizy, A.: J.Supercond. Nov. Magn. 23, 1325 (2010)

[10] N. A. Khan, S. H. Safeer, M. Rahim, M. N. Khan, and N. Hassan, "*Excess Conductivity Analysis of $Cu_{0.5}Tl_{0.5}Ba_2Ca_{n-1}Cu_nO_{2n+4-\delta}$ (n = 2, 3, 4) Thin Films,*" Journal of Superconductivity and Novel Magnetism, vol. 30, no. 6, pp. 1493–1498, Dec. 2016, doi: 10.1007/s10948-016-3942-z.

[11] N. A. Khan and S. Ahmad, "*Para-conductivity and critical regime of* $(Tl_{1-x}C_x)$ $Ba_2Ca_3Cu_4O_{12-\delta}$ *superconductors,*" Journal of Applied Physics, vol. 112, no. 3, p. 033912, Aug. 2012, doi: 10.1063/1.4740238.

[12] N.A. Khan, Fasih-ud-Din, A.A. Khurram, Phys. C Supercond. Its Appl. 417 (2005) 119– 126.

[13] S. H. Safeer, A. Raza, N. A. Khan, and M. N. Khan, "*Suppression of Superconductivity by Anharmonic Oscillations in Zn- or Ni-doped* $Cu_{0.5}Tl_{0.5}Ba_2(CaMg)Cu_{1.5}M_{1.5}O_{10-\delta}$ *(M=Zn, Ni) Superconductors; Evident by Magnetic Measurements*," Journal of Electronic Materials, vol. 50, no. 11, pp. 6518–6524, Sep. 2021, doi: 10.1007/s11664-021-09195-x

[14] Tominoto, K., Terasaki, I., Rykov, A.I., Mimura, T., Tajima, S.: Phys. Rev. B 60, 114 (1999)

[15] N. A. Khan, M. A. Rafique, M. Mumtaz, and G. Hussain, "*Investigation on Critical Regime of* $Cu_{0.5}Tl_{0.5}Ba_2(Ca_{2-x}Be_x)(Cu_2Ti)O_{10-\delta}$ *Superconductor via Excess Conductivity Analysis*," Journal of Superconductivity and Novel Magnetism, vol. 28, no. 11, pp. 3243–3248, Aug. 2015, doi: 10.1007/s10948-015-3185-4.

[16] N. A. Khan and S. Hussain, *"Enhanced superconductivity by Na doping in* $(Cu_{0.5}Tl_{0.25}Na_{0.25})$ $Ba2Ca_2Cu3O_{10-\delta}$," Journal of Alloys and Compounds, vol. 475, no. 1–2, pp. 652–657, May 2009, doi: 10.1016/j.jallcom.2008.07.091

[17] R. Awad, A. I. Abou-Aly, S. Isber, and W. Malaeb, "*Effect of the partial replacement of Ca by alkaline element Na on Tl-1223 superconductor*," Journal of Physics: Conference Series, vol. 43, pp. 474–479, Jun. 2006, doi: 10.1088/1742-6596/43/1/118.

[18] T. Aytug, A. A. Gapud, S. H. Yoo, B. W. Kang, S. D. Gapud, and J. Z. Wu, "*Effect of sodium doping on the oxygen distribution of Hg-1223 superconductors*," Physica C: Superconductivity, vol. 313, no. 1–2, pp. 121–126, Feb. 1999, doi: 10.1016/s0921-4534(98)00699-6

Chapter # 3

Synthesis and experimental techniques

This section illustrates the methodology of synthesizing samples and experimental techniques performed to study structural, optical and electrical properties of Na doped CuCaTl-1223 samples.

3.1 Synthesis of Tl-based High-temperature Superconductors:

When high-temperature superconductors (HTSC) are being synthesized, it is mandatory to use chemicals with 99% or better purity but this level of purity is not attainable. The formation of high-temperature ceramic superconductors doesn't show renowned enhancement in T_c because of surplus degrees of freedom, short coherence length (A), a natural inclination towards defects formation and inhomogeneity **[1]** .

Fundamental research and applications of high-temperature superconductors require samples with high phase purity. For example, the impurity phases within the superconducting grains impede the flow of electric current, resulting in a decrease in the electrical current density, Jc. This decrease in J_c enhances flux pinning. For this reason, the synthesis of these superconductors involves using a single phase. Secondary phases can be generated in a controlled manner by heating if desired. Tl-based superconductive oxides are commonly synthesized by reacting compounds in solid states. Various methods and techniques have been developed successively to avoid the use of off-stoichiometry initializing compositions in order to achieve diverse successful results **[2-8].** These methods have been used to synthesize the desired superconducting phases, which are formed either through a single step or a series of calcination steps. A distinct transitional product is formed after each calcination step. Under suitable calcination conditions, Tl-based high temperature superconductors can be synthesized with high phase purity in short calcination period **[9]**

3.1.1 Difficulties arise in phase control:

We needed off-stoichiometric initializing compositions for the following reasons:

- Incongruent melting
- • Thallium is lost as vapors during high-temperature calcination.

A new solid-phase whose stoichiometry differs from the composition of the superconducting sample can be generated by incongruent melting. Hence for the synthesis of Tl-based superconductors (single phase), from stoichiometric starting compositions, incongruent melting point (IMP) should be the upper limit of

temperature. Since incongruent melting occurs in a wide array of Tl-Ba-Ca-Cu amalgams so a small change in cation ratio could have a deep effect on final products and their distribution **[10]**. The loss of Tl occurs in form of Tl_2O fumes during high-temperature treatment. Below the melting point of Tl_2O_3 (712°C), Tl_2O vapors are formed by the decomposition of solid Tl_2O_3.

$$Tl_2O_3 = Tl_2O(g) + O_2(g)$$

Tl_2O vapor pressure can be expressed as **[11]**

$$log\, P = -19.36\left(\frac{10^3}{T}\right) + 18 \cdot 60$$

Here, P demonstrates vapor pressure of Tl_2O and T is temperature.

It is noted that Tl_2O_3 decomposes to Tl_2O, forming $Tl_2O_3 - Tl_2O$ mixture, above its melting point **[12].** As temperature increases, Tl_2O vapor density increases.

$$Tl_2O_3 - Tl_2O(\mathrm{I}) = Tl_2O_3(g) + \mathrm{x}O_2(\mathrm{g})$$

The boiling point of $Tl_2O_3 - Tl_2O$ is about 895°C **[13]** and this temperature is very similar to the one we used for the calculations. Stoichiometry and the phases of superconducting samples change due to the depletion of thallium. Thallium vaporizes at a slower rate from Tl-based superconductors but still, it can't be overlooked. The synthesis process of Tl-based superconductors has been carried out in closed vessels to reduce Tl loss. Samples are wrapped in a gold capsule. In certain cases, powdered thallium is placed near the samples as a source of Tl_2O vapors to lessen the loss of thallium. Alternatively, high oxygen pressure is also used to diminish thallium loss but it can change the stability of each superconductive phase.

3.2 Solid-state Reaction Method:

In this process, polycrystalline ceramic superconductors are synthesized using solid materials as reactants **[14]**. Firstly, all the reactants are ground together to improve the interaction between them. Since a considerable quantity of energy is required to overcome lattice energy so precursors are heated at high temperature. This given temperature supports the mobility of atoms at a high rate. The movement of atoms within the lattice is slow but it can be made rapid by increasing temperature **[15].** Solid-state reaction process is comprised of two main steps, calcination and sintering. Calcination involves breakdown of solid oxides into their respective elements and afterwards these elements are again combined to give a new product. Grain size and crystal structure of the product are improved by the sintering process.

3.3 Characterization Technique:

The experimental techniques done for the analysis for ceramic superconductors are mentioned in the figure below

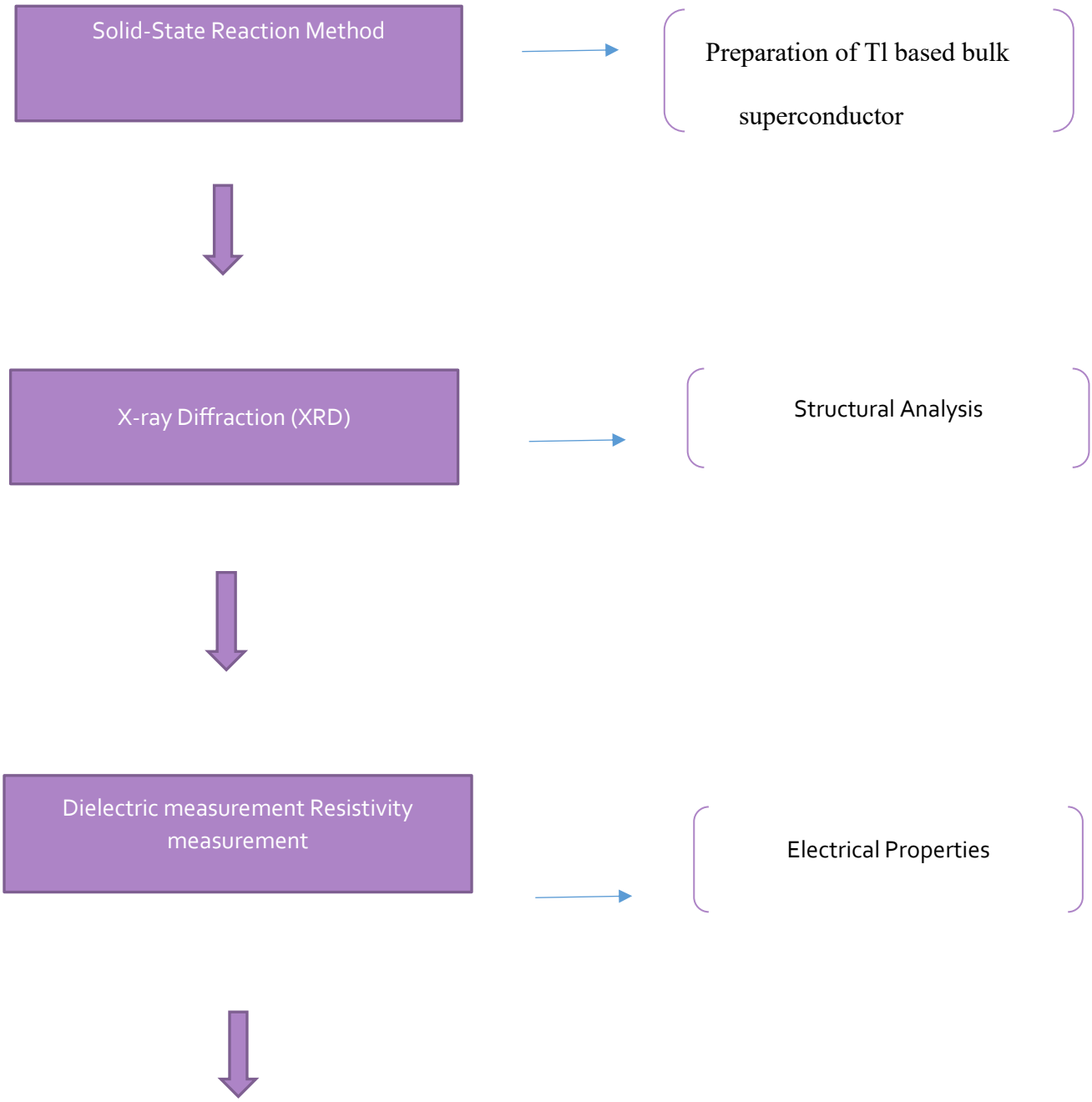

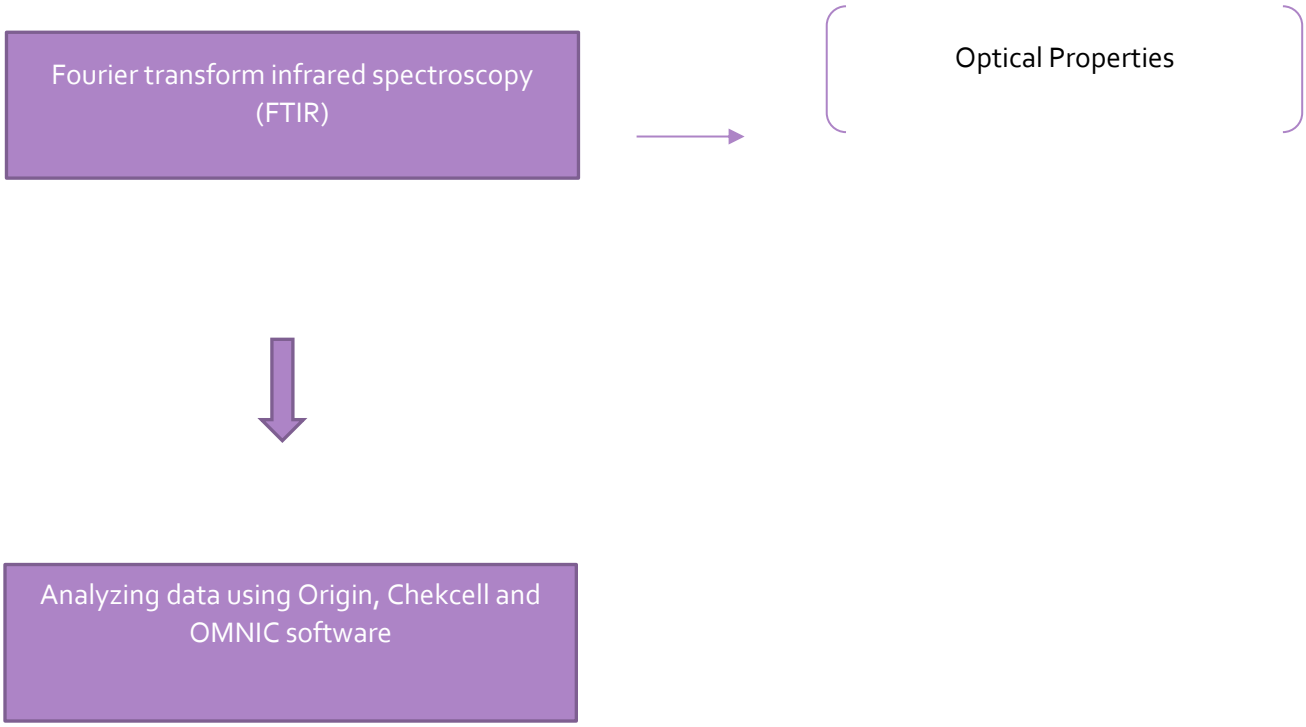

3.3.1 Diffraction of X-rays (XRD):

The XRD method is used to obtain information about the crystal structure of the sample which includes lattice parameters, stress, strain determination, phase analysis, defects, crystallite size. Diffraction can only take place if the wavelength of light shine on crystal structure is comparable to the spacing between planes. Since the wavelength of x-rays (10 nm) fulfils that condition so x-rays are used to study crystal structure. A crystal which can diffract x-rays possesses natural grating **[16]**.

3.3.1.1 Basic working principle of XRD:

XRD works on Bragg's law. It was first proposed by father and son duo (Lawrence Bragg and Henry Bragg). They discovered the reflection of x-rays from crystalline materials at a particular angle. X-rays are electromagnetic waves having high energy and small wavelength. The distance spanned by two parallel X-ray beams must be an integral multiple of λ being used for the diffraction of X-rays from the crystal, which is made up of parallel planes. This phenomenon is referred to as Bragg's law. An incident ray makes an angle θ with a crystal plane. For the path difference 'd' of these two X-rays,

Constructive interference can only occur between two reflected waves when their path difference is an integral multiple of their wavelengths. Hence, the condition for constructive interference is,

$$2d\sin\theta = n\lambda$$

Where n is a positive integer. Equation (3.2) is well-known Bragg's equation and it can determine d if the wavelength of x-rays is given. Analyzing crystal structure using Bragg's law has laid the foundation of x-ray crystallography **[17]**.

3.3.1.2 Methods used for x-ray diffraction:

Some of the methods are discussed below:

- Laue's Method

In this method, stationary crystal is being targeted by x-rays at a fixed incident angle. Only the wavelength of incident beams varies. These different wavelength beams reflect only through those crystal planes, whose geometry satisfies Bragg's law.

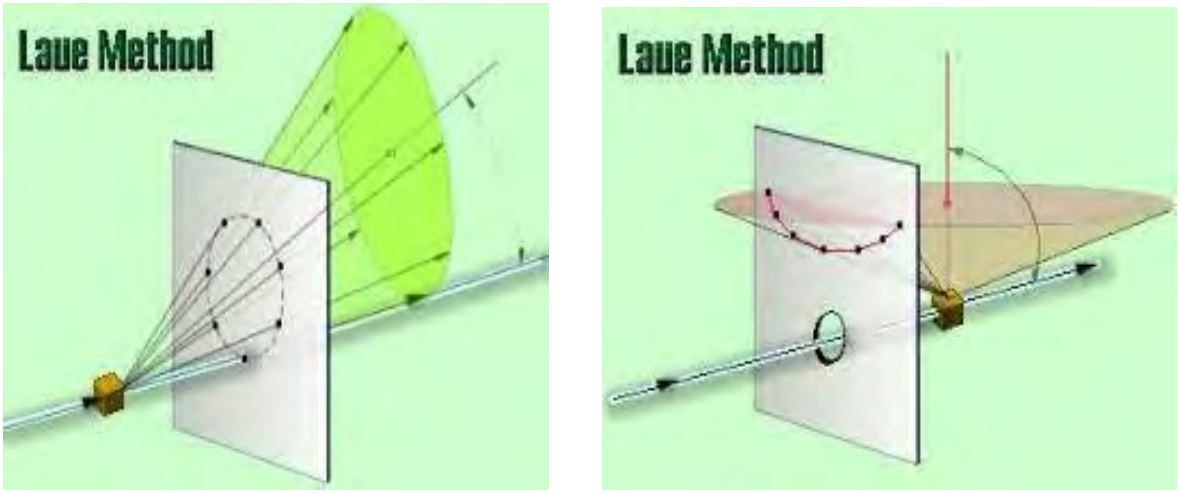

Laue's Transmission Method

- **Rotating crystal method:**

In this method, crystal is firstly placed normal to x-ray beam and then in a thin cylindrical film. After sparkling X-ray beam on the crystal, it begins to rotate about its axis. In this case, the wavelength of x-rays remains constant whereas the incident angle changes. Since x-rays are shone to different sets of planes but diffraction will occur from only those planes which make correct Bragg angle with incident x-rays

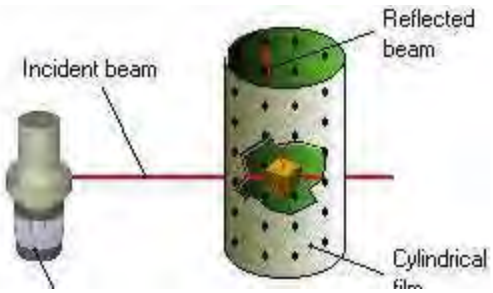

Figure 3.1 Determining the crystal structure by rotating sample

3.3.1.3 The X-ray diffractometer:

In X-ray diffractometer, x-rays are incident on material and then interacts with it producing a scattering pattern which helps in identifying crystal structure. The constituents of the x-ray diffractometer are:

- The X-ray sources
- The Sample holder
- The X-ray detector

Cathodes produce x-rays which are then filtered to produce monochromatic radiation. Mostly Mo and Cu target materials are used to produce x-rays having wavelengths 0.8A^{o} and 1.54A^{o} respectively **[18].** The phenomenon of diffraction occurs When the x-rays are emitted and focused onto the sample. Sample holder and x-ray detector both rotate continuously and the intensities of reflected x-ray beams are recorded by the counter. The x-ray source, sample and the counter are in the same plane. The counter rotates about its axis and its angular displacement is given by 2θ. The counter and the sample are set up so that if the sample rotates through an angle, the counter rotates through 2θ as a result. As a result, both the incidence angle and the reflection angle are kept constant.

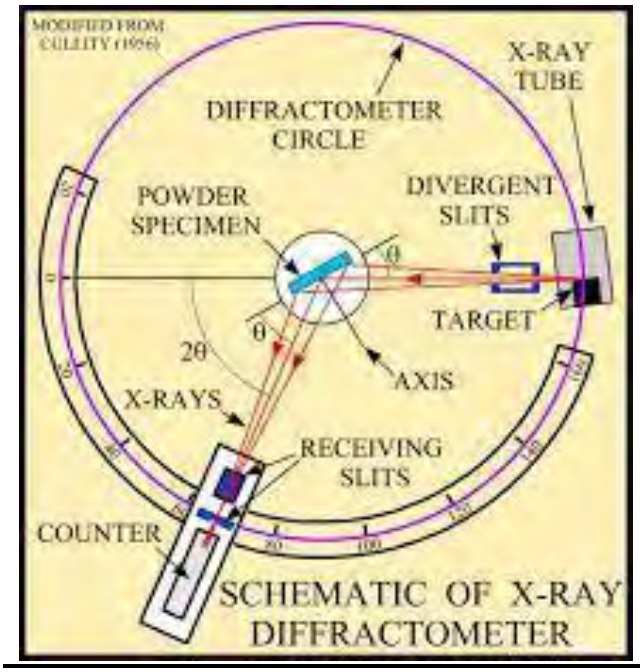

Figure 3.2 Schematic of X-ray Diffractometer

3.3.2: Resistivity Measurement:

Conductors, insulators and semi-conductors can also be classified based on band gap present between their conduction and valence bands. Insulators have a large band gap whereas semiconductors possess a narrow gap among valence and conduction band. But the valence and conduction band of conductors overlap. Applying potential difference across the ends of a conductor allows the flow of electrons from the valence band to conduction band. The resistivity of electrons due to the collisions with lattice atoms was expressed by the Drude model as:

$$\rho = \frac{m}{n\tau e^2}$$

Resistivity dependence on mean free time τ

Free electrons begin to flow in metal through the use of an outside electric field and as a result, current flows through the metal. At T=0, ions do not scatter the electrons because they are regularly arranged in the lattice but impurities and dislocations within the lattice of crystals are responsible for scattering of electrons. Since real metals possess impurities and lattice imperfections so even at the low temperature, they resist the flow of electrons. The resistivity due to lattice imperfections at T=0 is called residual resistivity „ ρ_i. Lattice atoms begin to undergo thermal vibrations on increasing temperature. These lattice vibrations also

cause resistance in the flow of electrons and this resistivity is named as phonon resistivity „ ρ_{Ph}" **[19].** Hence the electrical resistance depends on mean free time due to:

- Dispersion of electrons from lattice defects i.e. impurities.
- Electron scattering from thermal lattice vibrations i.e. scattering due to phonons.

Therefore, resistivity is articulated as

$$\rho = \rho_i + \rho_{Ph}$$

3.3.2.1 Resistivity dependence on temperature:

The increase in temperature results in the increase in lattice vibrations' amplitude which is responsible for enhancing the collisions among electrons and lattice vibrations (phonons), these collisions then upturn the resistivity. In contrast, these collisions reduce at low temperatures and so does the resistivity. The dependence of resistivity on temperature is of the order of T^5 at low temperatures, which is experimentally proved for alkali metals **[20].** At high temperature, resistivity is proportional to the mean square amplitude of phonons.

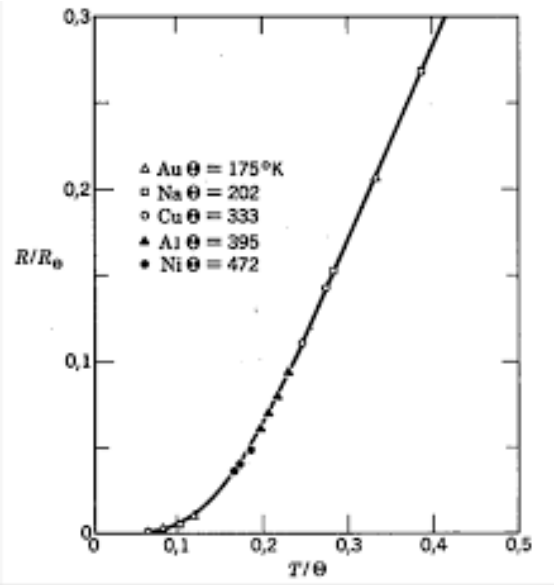

Figure 3.3 Resistivity dependence of normal metals on temperature

3.3.2.2 Four-probe Method:

The resistivity of metals, semiconductors and superconductors is measured using the four-probe method. It is ideal than the two-probe method because in the later method error arises due to the contact resistance of leads. The two-probe method can measure resistivity only up to Ohms whereas four-probe method can

measure up to milli Ohms and micro Ohms. In the four-probe method, four equidistant contacts are made on the flat superconducting sample's surface with the help of silver paste. Silver paste makes good quality contacts so they don't break even if the sample is cooled at very low temperature. The two outer contacts allow the flow of current from the superconducting surface whereas the two inner contacts are for the passage of voltage through the sample

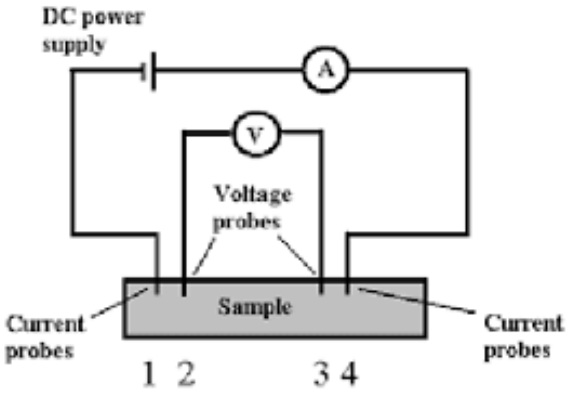

Figure 3.4 Diagram exhibiting four-probe method's setup

For the resistivity measurement from this method, we take 1 mA current. Liquid nitrogen is used for cooling samples because superconductivity arises below room temperature. A thermocouple is used for sensing temperature. The resistivity of the sample can be found by using the relation

$$\rho(T) = \frac{A}{L}\frac{v}{I}$$

Steps for taking measurements using the four-probe method are

- Liquid nitrogen was put in a simple cryostat and a sample holder, made up of brass, was fitted from one end with sample whereas its other end was attached with wires.
- MW2122A regulated DC power supply was connected in series with the resistance as a source of constant current.
- The change in voltage arose due to the variation in temperature was measured by P2000/E KEITHLEY MULTIMETER.
- Thermocouple measured the temperature in milli-volts.

- The current was measured up to 1A with least count of 1milli A by an ammeter attached in series with the resistance

3.3.3: Fluctuation Induced Conductivity (FIC) analysis:

A method for analyzing superconductor fluctuations is referred to as a "para conductivity analysis" and is a result of the formation and destruction of Cooper pairs at temperatures lower than the onset. Cooper pairs begin to form above the transition temperature, but thermal fluctuations cause them to form and annihilate until the critical temperature (Tc) is reached, at which point the resistance becomes zero (R=0). The density of fluctuation decreases as we cool our sample below T_c(R=0), where thermodynamic fluctuation cannot significantly obstruct the formation of cooper pairs. Condensation of Cooper pairs consequently occurred, resulting in zero resistance**.** These fluctuations that induced conductivity exhibit for a temperature regime near T_c known as Ginzburg temperature (T_G). For low temperature superconductors the value of T_G is less than 1 μK whereas it is around (1 – 2) K for the HTSCs. Therefore, it is possible to analyze these fluctuations. Ginzburg was the first scientist who probe the contribution of fluctuations to heat capacity and formulate the value of temperature where fluctuation modification to heat capacity is important as determine by relation below

$$\frac{\Delta T}{Tc} \sim \left(\frac{Tc^4}{\varepsilon_f}\right) \sim \left(\frac{a^4}{\xi}\right) \sim 10^{-4} to\ 10^{-6}$$

Here 'ξ' represents coherence length and 'a' represents inter-atomic separation between two lattice sites. The value of $\Delta T/T_c$ is so small therefore these fluctuations were undetectable experimentally for a long time. Due to the variation that caused conductivity to deviate noticeably at higher temperatures from its linear dependency, given as.

$$\Delta\sigma(T) = \frac{\rho_N(T) - \rho_1}{\rho_1 N(T)\rho(T)} T$$

Here the ρ(T) denotes actual resistivity and a $\rho_N(T) = \alpha + \beta T$ represent a normal state extrapolated resistivity. Two distinct types of fluctuation are typically regarded as: The first is the Aslamazov-Larkin (AL), which is linked to excess current that develops as a result of Cooper pair oscillations at temperatures higher than T_c. The second one, a Maki Thompson (MT) contribution, discussed how superconducting carrier fluctuations affected the conductivity of ordinary electrons. The crossover point between a three-dimensional (3D) electronic state and a two-dimensional (2D) electronic state is shown by a different model called the Lawrence-Doniach (LD) model. The 'MT' term has a dependence on phase-relaxation time 't_φ' and exhibits a large effect in the 2D fluctuation area for moderate pair breaking, whereas the 'AL' term is found close to 'T_c'. Hence, the FIC offers insightful data regarding the superconductor's dimensionality,

phase relaxation time t_{φ}, and coherence length $\xi_c(T)$. The analysis of crossover temperatures by using LD model have been testified by various researchers but here the MT contribution didn't convince many researchers because of their lack of possibility to evaluate τ_{φ}. FIC analysis of polycrystalline bulk material is mainly consistent with the characteristic of 3D fluctuation, but the results are bit different from thin films and here 3D to 2D crossover has been observed in thin films with strong c-axis orientation. The superiority of 3D fluctuations or 2D-3D crossover is temperature dependent. Different experimental results have been discovered in the case of a single crystal.

3.3.3.1 Fourier Transform Infrared Spectroscopy (FTIR):

In solid, atoms of materials vibrate with frequency about their mean positions. These vibrations depend on the mass of atom, bond angle and bond length. Even at 0K temperature, atoms vibrate. Lattice vibrations are very necessary to explain the physical properties of the materials. For characterization, we need to determine which type of vibrational modes are present in a given material.

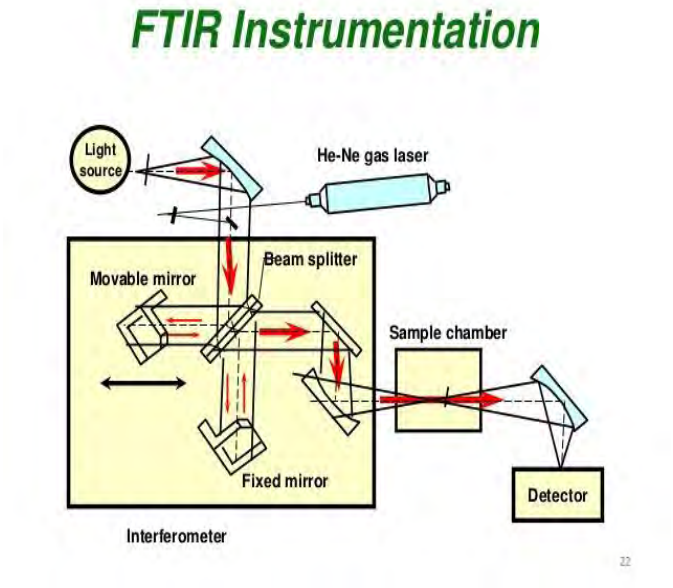

Figure 3.5 The diagram of FTIR instrument

We employ a method called Fourier transform infrared radiation (FTIR) spectroscopy to find these modes.

3.3.3.2 Components of FTIR:

The main component of FTIR are,

- Michelson Interferometer
- Light source or laser
- Sample
- Detector
- Computer

Michelson interferometer:

Michelson interferometer is important part of FTIR spectrometer. Michelson Interferometer contains,

- A moving mirror
- A fixed mirror
- Detector
- A beam splitter

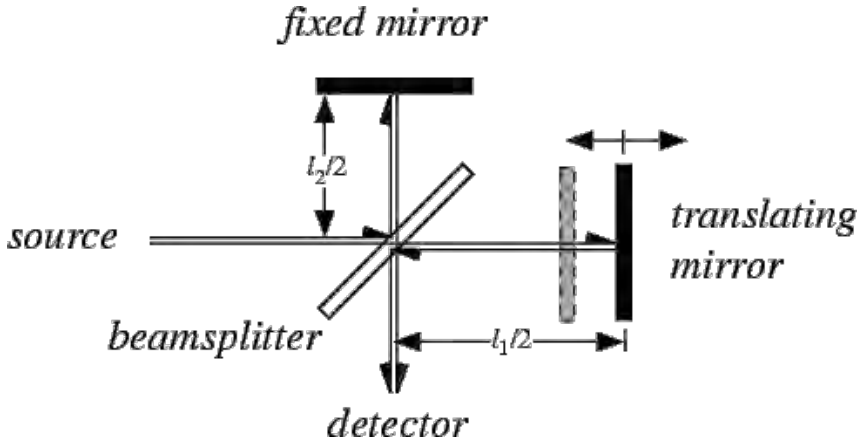

Figure 3.6 Michelson interferometer

Moving and fixed both mirrors are mutually orthogonal. Whereas the beam splitter is placed in the center of interferometer whose function is to split incident infrared radiation into two equal parts. Half of incident beam is reflected towards a fixed mirror whereas the other half gets transmitted towards the moving mirror. The two split beams then recombine at beam splitter after reflection. The phase difference arises due to the

translation of moving mirror results in the formation of the interference pattern on the 60 recombination of these beams. The intensity of the reflected beam is maximum at 0o phase difference and minimum at 180o phase difference. The resultant beam focused on the sample and sensed by the detector produces a sinusoidal interferogram (absorption spectrum in the time domain) because of the moving mirror. Fourier transformation is then applied to interferogram to convert it from the time domain to the frequency domain. This interferogram contains the information about frequency absorbed by the sample and detector

3.3.3.3 The source:

Infrared rays are emitted from a radiant source in a beam. This beam (rays) passes through the gap to regulate the quantity of energy that enters the sample and eventually reaches the detector.

3.3.3.4 Procedure:

In order to study the modes of vibrations in superconducting samples, the FTIR spectrum has the following steps,

- We used OMNIC software to analyses the studied spectrum of our samples.
- KBr pellet was made and its spectrum was set as a background spectrum, the range of spectrometer was set from 400 cm^{-1} to 700 cm^{-1} undergoing 200 scans for taking spectrum.
- We added approximately 5 mg of superconductor in 50 mg KBr compound, mixed them properly and made the pallet. Again, we took 300 scans of the mixed sample spectrum and range was already set at 400-700 cm^{-1}.
- As we used KBr as background and after subtracting the background spectrum, the computer only displayed spectrum of our sample.

References:

[1] Allen M. Hermann, Thallium-Based High-Temperature Superconductors, Marcel Dekker, Inc. (1994) p 41.

[2] C.C. Torardi, Science 240, 631 (1988).

[3] N.L. Wu, Mater. Lett. 7, 169 (1988).

[4] N.L. Wu, Jpn. J. Appl. Phys. 28, L1349 (1989).

[5] N.L. Wu, Physica C 161, 302 (1989).

[6] E. Ruckenstein and C. T. Cheung, J. Mater. Res. 4, 1116 (1989).

[7] E. Ruckenstein and S. Narain, Mater. Lett. 8, 421 (1989).

[8] P. Barboux, J. Appl. Phys. 63, 2725 (1988).

[9] N.P. Ong, R. J. Cava, Science 305, 52 (2004).

[10] K. C. Goretta, Mater. Res. Bull. 25, 791 (1990).

[11] D. Cubicciotti and F. J. Keneshea, J. Phys. Chem. 71, 808 (1967).

[12] A. b. F. Duncan, J. Am. Chem. Soc 51, 2697 (1929).

[13] K. Wade and A. J. Banister in Comprehensive Inorganic Chemistry Vol 1Pergamon Press London (1973) p 1146.

[14] M. Paulus and P. Hagen Muller, Preparative methods in Solid State Chemistry, Academic Press, New York, 487 (1972).

[15] I. Parkin, Chemical Society Reviews 25(3), 199 (1996).

[16] J.S. Blakemore, Solid State Physics, Cambridge University Press, (1985).

[17] W.H. Bragg and W.L. Bragg, Proc. R. Soc. Lond. A 88, 428 (1913).

[18] B.E. Warren, X-ray Diffraction, Dover Publications, (1969)

[19] M.N. Rudden and J. Wilson, Elements of Solid State Physics, 2nd edition (1993).

[20] K.L. Horouitz and V.A. Johnson, Academic Press, New York and London, 401 (1959

CHAPTER # 4

Results and Conclusion

4.1 introduction:

Low-dimensional, high-Tc superconductors have a charge reservoir layer (CRL) that is made up of a carrier-supplying $Cu_{0.5}Tl_{0.5}Ba_2O_{4-\delta}$ layer having one or more $nCuO_2$ conducting-planes (for n=2,3,4,5,... etc.). $Cu_{0.5}Tl_{0.5}Ba_2Ca_2Cu_3O_{10-\delta}$ (CuTl-1223) superconductor (with n=3) of $nCuO_2$ has highest critical-temperature **[1-5].** The conductive CuO_2 planes receives carriers from the charge reservoir and the superconductivity is exhibited in planes. In our previous studies, we have established that the mechanism of high T_c superconductivity involves a definite contribution of small spins of copper atoms in the $3d^9$ position in the CuO_2 plane. We reached at such conclusion by doping spin-less Zn ($3d^{10}$) at planar CuO_2 sites. Since the high conductivity in the two-dimensional junction leads to CuO_2 planes, the phase coherence in different conduction planes will determine the final critical temperature. Therefore, it is necessary to study such phase coherence and determine the Ca atoms in the space between the planes. In the current research, we study $Cu_{0.5}Tl_{0.5}Ba_2(Ca_{2-x}Na_x)\ Cu_3O_{10-y}$ (x=0, 0.25, 0.5, 1) samples by doping Na atoms $Cu_{0.5}Tl_{0.5}Ba_2(Ca_{2-x}Na_x)\ Cu_3O_{10-y}$ (x=0, 0.25, 0.5, 1) Calcium atoms in cells are in the natural Ca^{+2} oxidation state, while sodium atoms are in Na^{+1} state of charge. The increase of Na doping in the later compound will reduce the interplanar bonding that in turn would decrease the phase coherence among carriers in different CuO_2 planes. This study will determine the role of long-range phase coordination in determining the final critical temperature of superconductivity in these substances. Additionally, the part of atomic charge states between CuO_2 planes will be established. The Y^{+3} is required for better interplane coupling in the $YBa_2Cu_3O_7$ superconductor for optimal critical temperature. In $YBa_2Cu_3O_7$ samples, the role of Y^{+3} is taken over by Ca^{+2} in the homologous phase of $Cu_{0.5}Tl_{0.5}Ba_2(Ca)Cu_2O_{8-y}$ sample. Therefore, it is important to determine the possible charge state's function of the atoms between the planes of CuO_2 in such samples.

4.2 Test Approach:

The sodium doped sample with a concentration of x=0, 0.25, 0.5, 1 in CuTl 1223 sample were prepared by two-step method of solid-state reactions**.** In the initial stage, substances like $CaCO_3$, Ba $(NO_3)_2$, NaOH and $Cu_2(CN)_2 + H_2O$ were ground for about 1h in pestle & mortar to determine the composition of the reactants.

For a 24-hour period, the ground material was heated by being fired, twice, at 860 °C in quartz boats inside a preheated chamber furnace. The furnace was then cooled to room Temperature (300K). In the second step, the calculated amount of Tl_2O_3 added to the fired precursors and mixed for about 30 minutes. Thallium mixed material is then palletized under a pressure of 5 tons/cm^2 and pellets are placed in a gold capsule and heated for 12 minutes at 860ºC in a chamber furnace. X-ray diffraction (XRD), temperature dependent four probe resistivity measurements, dielectric properties, and FTIR measurements were used to characterize the produced samples. CuKα radiations with a wavelength of 1.54056Å were used in an X-ray diffraction scan to evaluate the structural phases of the materials, and the Checkcell computer program was used to determine cell parameters. The four-probe approach was used to calculate the sample's temperature-dependent resistance. NICOLET 5700 was used to measure the 400-700cm-1 wavenumber's range of FTIR absorption spectra. The KBr pallets were used to obtain the background spectra of the samples.

4.3 Advice and Speech:

4.3.1 The X-ray analysis:

Figure 4.1: The XRD of $Cu_{0.5}Tl_{0.5}Ba_2(Ca_{2-x}Na_x)\ Cu_3O_{10-y}$ (x = 0, 0.25, 0.5, 1)

The X-ray diffraction scan for the sample of $Cu_{0.5}Tl_{0.5}Ba_2(Ca_{2-x}Na_x)\ Cu_3O_{10-y}$ (x=0, 0.25, 0.5, 1) in CuTl 1223 are shown in Figure 4.1. The dominant CuTl-1223 superconducting phase is observed in this diffraction pattern. There is a maximum number of indexed X-ray diffraction lines in the orthorhombic crystal structure that followed the P4/mmm space group. Some low intensity non-indexed diffraction lines marked with symbol **(*)** are impurity lines belonging to $BaCuO_2$ and Ba_2CuO_3 phases.

Fig 4.2(a) comparison of the samples on the b-a axis with sodium doped sample with a concentration of x=0, 0.25, 0.5, 1 in CuTl 1223

c- axis

Fig. 4.2(b): Comparison of the c-axis and volume with sodium doped sample with a concentration of x=0, 0.25, 0.5, 1 in CuTl 1223

The orthorhombic distortion observed in b-a axis increases in all Na-doped samples, Fig. 4.2(a), while Na doping at Ca sites increases the c-axis length, Fig. 4.2(b). This is a significant feature of Na doping in the final compound that increased Na-doping results in the elongation of CuO_2 planes, which would suppress the phase coherence of the carriers. It is expected that the resistivity at room temperature of Na-doped samples would increase and their critical temperature will decrease as a possible consequence of suppression of the phase coherence of the carriers in different planes of CuO_2.

Sr	Sample	a-axis(A)	b-axis(A)	c-axis(A)	Volume(A^3)
1	$Cu_{o.5}Tl_{0.5}Ba_2Ca_2Cu_3O_{10-y}$	3.884	3.963	14.50	223.2
2	$Cu_{o.5}Tl_{0.5}Ba_2Ca_{1.75}Na_{0.25}Cu_3O_{10-y}$	3.852	3.928	14.53	219.8
3	$Cu_{o.5}Tl_{0.5}Ba_2Ca_{1.5}Na_{0.5}\ Cu_3O_{10-y}$	3.823	3.890	14.59	216.9
4	$Cu_{o.5}Tl_{0.5}Ba_2Ca_1Na_1Cu_3O_{10-y}$	3.752	3.830	14.66	210.7

Table 4.1: $Cu_{0.5}Tl_{0.5}Ba_2Ca_{2-x}Na_xCu_3O_{10-y}$ (x=0, 0.25, 0.5, 1) lattice parameters

4.3.2 Resistivity measurement:

The resistivity versus temperature measurements of $Cu_{0.5}Tl_{0.5}Ba_2(Ca_{2-x}Na_x)\ Cu_3O_{10-y}$ (x=0, 0.25, 0.5) samples are shown in Fig.4. 3(a); samples with $Cu_{o.5}Tl_{0.5}Ba_2Ca_1Na_1Cu_3O_{10-y}$ showed semiconducting behavior that followed variable range range hopping conductivity. $Cu_{0.5}Tl_{0.5}Ba_2(Ca_{2-x}Na_x)\ Cu_3O_{10-y}$ (x=0, 0.25, 0.5) samples have shown onset of superconductivity around [Tc(onset)] at 106.6, 108, 109K and the zero-resistivity critical temperature 101, 96.5, 99.7K, respectively.

Fig 4.3: (a) $Cu_{0.5}Tl_{0.5}Ba_2Ca_{2-x}Na_xCu_3O_{10-y}$ (x=0, 0.25, 0.5) resistivity patterns

The magnitude of the resistivity increases with increased Na-doping on the Ca sites and finally becomes semiconducting in the $Cu_{o.5}Tl_{0.5}Ba_2Ca_1Na_1Cu_3O_{10-y}$ samples. It is most likely that the calcium state changes from Ca^{+2} in undoped samples to Ca^{+2}/Na^{+1} in doped samples that most likely increases the decoupling of the CuO_2 plane. Such decoupling of CuO_2 planes would in turn limit the phase coherence of the carriers. In $Cu_{o.5}Tl_{0.5}Ba_2Ca_1Na_1Cu_3O_{10-y}$ samples some asymmetric processes are induced which eventually make the material semiconducting, Fig.4.3b.

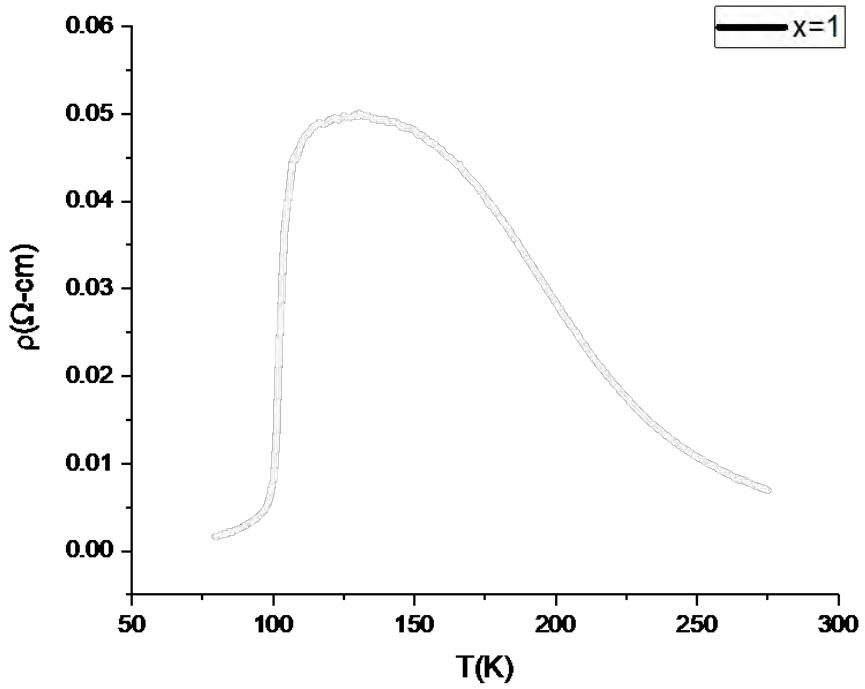

Fig 4.3(b) temperature Vs resistivity graph for semiconducting sample $Cu_{0.5}Tl_{0.5}Ba_2Ca_1Na_1Cu_3O_{10-y}$

Samples $Cu_{o.5}Tl_{0.5}Ba_2Ca_1Na_1Cu_3O_{10-y}$ showed variable range hopping (VRH) conductivity, which follows a relation of the form:

$$\rho(T) = \rho_o \exp\left[\left(\frac{T_o}{T}\right)^{1/4}\right] \qquad (12)$$

The ρ–T data of different samples were evaluated using the Mott 3D VRH type conduction method (with b = 1/4) **[6].** The Mott 3D VRH model is a good fit to the results of our $Cu_{o.5}Tl_{0.5}Ba_2Ca_1Na_1Cu_3O_{10-y}$samples. $Cu_{o.5}Tl_{0.5}Ba_2Ca_1Na_1Cu_3O_{10-y}$ has a semiconductor-like resistivity variation that fitted to Mott 3D VRH model in the temperature region of 77K to 300K. In Fig.4.3(c) is shown the resistivity fitted to the Mott 3D VRH model and in the inset of it is displayed ln ρ vs represents a plot of $1/T^{1/4}$ that followed the Mott Varying Range Hopping (VRH) conductivity. The energy of activation for thermally activated processes is shown by a straight line that gave its value around 4.2 meV.

Fig.4.3(c) $Cu_{0.5}Tl_{0.5}Ba_2Ca_1Na_1Cu_3O_{10-y}$ sample's activation energy curve

4.3.3 Fourier Transform Infrared spectroscopy measurements:

Fig 4.4: $Cu_{0.5}Tl_{0.5}Ba_2Ca_{2-x}Na_xCu_3O_{10-y}$ (x=0, 0.25, 0.5, 1) samples' FTIR absorption spectra

FTIR absorption analysis of sodium doped sample with a concentration of x=0, 0.25, 0.5, 1 in CuTl 1223 samples are shown in Fig.4.4. Two apical oxygen atoms of type Tl-OA-Cu(2) and Cu (1)-OA-Cu(2) are observed at (420–450)cm^{-1} and (480–540)cm^{-1} in the phonon's modes related to the vibrations of different O_2 atoms in the wavenumber range of 400-600 cm^{-1} , as well as a CuO_2 planar oxygen mode at 580 cm^{-1}. Here, the Cu(2) atom is in the superconducting plane and the Cu (1) atom is in the layer that stores charge. The CuO_2 planar oxygen mode observed around at 580 cm^{-1}, the apical oxygen modes of types Cu (1)-O_A-Cu (2) and Tl-O_A- Cu (2) are softened with the increased Na-doping in the sample. This is a clear manifestation of the change in dipole moment of samples with increased Na-doping. The change in dipole movement is supported by the increased c-axis length.

4.3.4 Fluctuation-induced conductivity analyses:

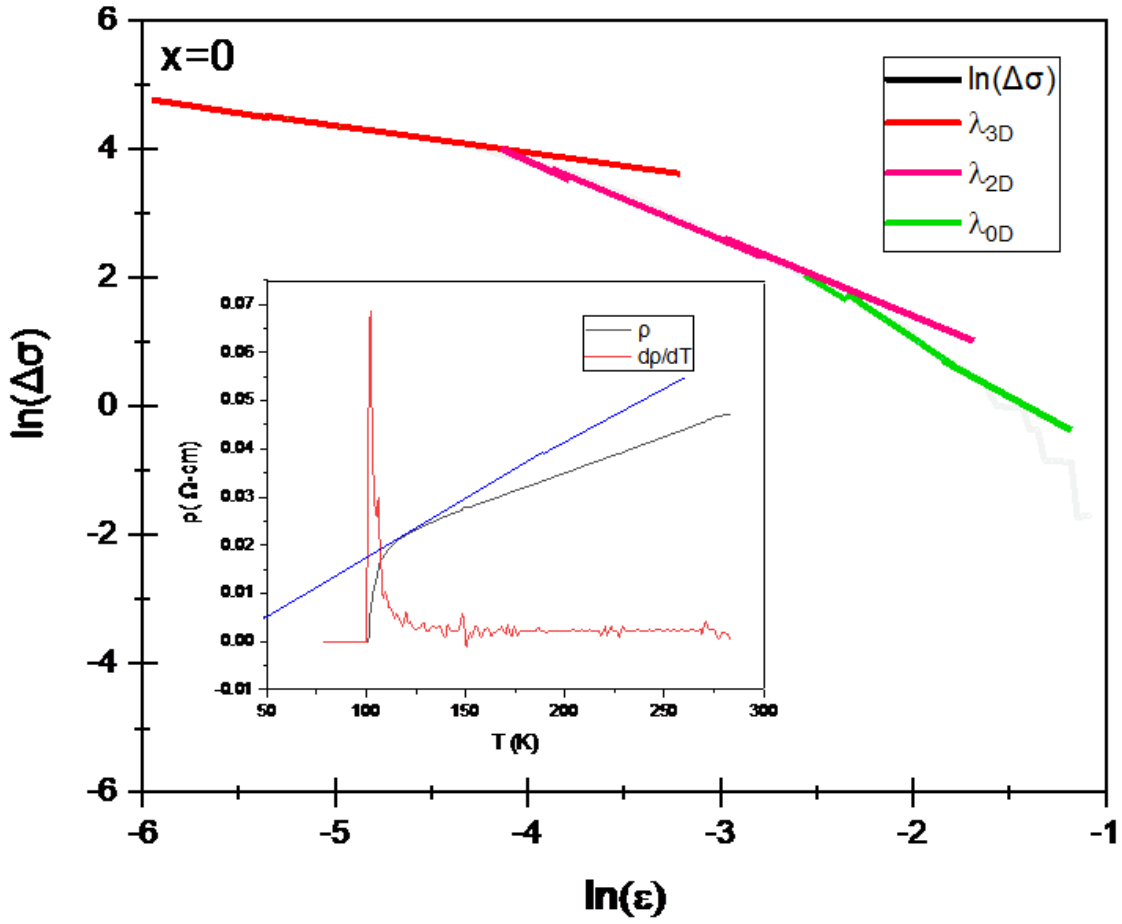

(a)

(b)

(c)

Fig 4.5(a,b,c): ln$\Delta\sigma(T)$ and ln ε plot for the samples $Cu_{0.5}Tl_{0.5}Ba_2(Ca_{2-x}Na_x)Cu_3O_{10-y}$(x=0, 0.25, 0.5)

The excess conductivity analysis of conductivity data is carried out for the studies of effect of doped Na atoms on the intrinsic superconductivity parameters. For such analyses, the Aslamazov Larkin (AL) model was used for thin films samples and a correction to it for the polycrystalline samples was proposed by Lorence Doniach (LD). Following the equation of the form $\Delta\sigma(T) = \Delta\sigma RT\varepsilon^{-\lambda D}$ in the temperature range around and beyond Tc gives these results. It is possible to rewrite this equation as follows:

$$ln\Delta\sigma_{(T)} = ln\Delta\sigma_{RT} - \lambda_D ln(\varepsilon) \quad \ldots\ldots\ldots\ldots\ldots\ldots \quad (1)$$

The $\varepsilon = \left(T - T_c^{mf}\right)/T_c^{mf}$ is lower temperature and λ_D is a dimensional exponent with a range of 0.3 to 2.0.

The λ_D around 0.3 corresponds to the critical exponent, λ_D around 0.5 to the three-dimension (3D), λ_D value around 1.0 to the two-dimensional (2D), and λ_D value equal to 2.0 to the zero-dimension (0D) conductivity. The Lawrence and Doniach (LD) model for the polycrystalline samples reads:

$$\Delta\sigma_{LD} = [e^2/16\hbar d](1 + J\varepsilon^{-1})^{-1/2}\varepsilon^{-1} \ldots\ldots\ldots\ldots\ldots\ldots (2)$$

In this equation, the thickness of the superconducting layers is d, which is equal to (~15 Å for CuTl-1223 samples), and $J = \left[2\xi_{c(0)}/d\right]^2$ is inter-layer coupling. The analyses of the excess conductivity's log plots against its reduced temperature, which result in the temperature transitions for thermally active processes resulting various cross over temperatures such as T_G, $T_{3D\text{-}2D}$, and $T_{2D\text{-}0D}$, as shown in Table 4.2. The mean field critical temperature is T_c^{mf} that is determined from dρ/dT, Fig.4.5(a,b,c). The T^{cmf}, $T^{3D\text{-}2D}$, $T^{2D\text{-}0D}$ and T_G are enhanced in all doped samples. According to LD model, the $\xi_{c(0)}$ (length of coherence along the c-axis) is $\xi_{c(0)} = \frac{d}{2}\left[\frac{T_{3D-2D}}{T_c^{mf}} - 1\right]^{1/2}$; the $T_{3D\text{-}2D}$ is cross over temperature**[7].** The intersection of various dimensional exponents determines the temperatures at which different thermally activated processes cross-over. The λ_{cr} refers to the slope below T_G, λ_{3D} above T_G, the λ_{2D} to the slope value above $T_{3D\text{-}2D,}$ and λ_{0D} corresponds to the slope of exponent value 2. The value of coherence length along the c-axis $\xi_{c(0)}$ so determined is used to calculate the Fermi velocity V_F and the phase relaxation time by using the following expressions

$$v_F = 5\pi k_B T_c \xi_{c(0)}/2K\,\hbar \ldots\ldots\ldots (3)$$

$$\tau_\varphi = \pi\hbar/k_B T_{2D-0D} \ldots\ldots\ldots (4)$$

K is the proportionality coefficient with a value of 0.12 as mentioned in the reference **[8].** The inter-CuO_2-plane coupling J and the energy needed to separate the Cooper pairs E_{Break} are determined by using phase relaxation time,

$$J = \frac{\hbar\tau\phi^{-1}}{2\pi k_B T} \ldots\ldots\ldots (5)$$

$$E_{Break} = \frac{h}{(1.6\times10^{-19})}(eV) \qquad \ldots\ldots\ldots (6)$$

Sample	λ_{CR}	λ_{3D}	λ_{2D}	λ_{0D}	$T_{CR-3D} = T_G$ (K)	T_{3D-2D} (K)	T_{2D-0D} (K)	T_c^{mf} (K)	T^* (K)	$\alpha = \rho_n(0K)$ (Ω-cm)
x=0	-	0.42	1.25	2.02	102.3	103.4	112.4	98	113.4	0.006
x=0.25	-	0.51	1.31	2.37	102	104	112.2	98.5	120.2	0.01
x=0.5	-	0.43	1.13	2.10	104.6	105.36	121.41	100.1	128.5	0.08

Table 4.2(a): superconducting parameters from the plot of ln$\Delta\sigma(T)$) and ln ε of sodium doped sample with a concentration of x=0, 0.25, 0.5 in CuTl 1223

Sample	$\xi_c(0)$ (Å)	J	N_G	$\lambda_{p.d}$ x 10^2 (Å)	$B_{c(0)}$ (T)	B_{c1} (T)	B_{c2} (T)	κ	$J_{c(0)}$ x 10^3 (A/cm^2)	V_F x 10^7 (m/s)	E_{Break} (eV)	τ_φ x 10^{-13} (s)
x=0	1.2	0.1	0.04	3.4	4.2	0.4	128	21.4	6.7	1.0	0.02	2.4
x=0.25	1.2	0.1	0.03	3.3	4.4	0.5	128	20.6	7.3	1.0	0.02	2.2
x=0.5	1.1	0.04	0.03	3.0	4.8	0.5	128	18.8	8.7	1.0	0.04	1.1

Table 4.2(b): Superconducting-parameters calculated from the FIC of $Cu_{0.5}Tl_{0.5}Ba_2$ $(Ca_{2-x}Na_x)$ Cu_3O_{10-y} (x=0, 0.25, 0.5) samples respectively

The values of the Fermi velocity V_F, the phase relaxation time, and the inter-layer coupling J, and the coherence length along the c-axis of the carriers are not significantly altered by Na-doping in the final compound, as shown in Table 4.2. The coherence length along the c-axis is related to the Fermi-vector via relation $K_F = [3\pi^2 N/V]^{1/2}$ and its magnitude is not significantly altered with Na-doping. It shows that superconducting carrier's density is not significantly altered in the final compound with Na-doping. The suppression of the critical temperature of the material and finally turning into a semiconductor like material indicated that somehow the phase coherence of the carriers in different CuO_2 planes is significantly reduced. These results have also demonstrated that the suppression of the zero-resistivity critical temperature not related to the suppression in the density of carriers but it is related to the suppression of phase coherence of the carriers in various conducting CuO_2 planes.

Ginzburg number N_G is determined at the cross-over point of critical regime and the three-dimensional regimes. The critical regime and the 3D-conductivity regimes crossover temperature is T_G. By using the T_G and N_G in the Ginzburg-Landau theory the following superconductivity parameters are determined by employing the following equations.

$$N_G = \left[\left(T_G - T_c^{mf}\right)/T_c^{mf}\right] = [1/2]\left[k_B T_c / B_{c(0)}^2 \gamma^2 \xi_{c(0)}{}^3\right]^2 \ldots\ldots (7)$$

$$B_{c(0)} = \Phi_0/2\left(\sqrt{2}\right)\pi\lambda_{pd}\xi_{ab(0)} \ldots\ldots\ldots (8)$$

$$B_{c1} = B_{c(0)} \ln\kappa/\left(\sqrt{2}\right)\kappa \ldots\ldots\ldots (9)$$

$$B_{c2} = \left(\sqrt{2}\right)\kappa B_{c(0)} \ldots\ldots\ldots \quad (10)$$

$$J_c = 4\kappa B_{c1}/3\left(\sqrt{3}\right)\lambda_{pd} ln(\kappa) \ldots. (11)$$

The superconductor anisotropy is given by equation $\gamma = \xi_{ab(0)}/\xi_{c(0)} = 5/(n-1)$ where n is a number of superconducting planes; for CuTl-1223 samples n = 3. In comparison with un-doped samples the values of $B_{c0}(T)$, $B_{c1}(T)$, and $J_c(0)$ are not significantly altered in Na-doped samples showing that the population of inadvertent defects are not significantly changed. The values of London penetration depth and the Ginzburg-Landau (GL) parameter $\kappa=\lambda/\xi$ in Na-doped samples are, therefore, not altered with Na-doping in the final compound. These analyses showed the significance of phase coherence of the carriers and decoupling in various CuO_2 planes suppresses superconducting properties in Na-doped samples.

4.3.5 Conclusions:

$Cu_{0.5}Tl_{0.5}Ba_2 (Ca_{2-x}Na_x) Cu_3O_{10-y}$ (x=0, 0.25, 0.5, 1) samples are synthesized at normal pressure and their superconducting properties are studied by XRD, resistivity measurements, FTIR absorption measurements.

$Cu_{o.5}Tl_{0.5}Ba_2Ca_1Na_1Cu_3O_{10-y}$ sample displayed variable range hopping conductivity with band gaps of 4.2meV. The transition temperature of superconductivity of $Cu_{o.5}Tl_{0.5}Ba_2$ $(Ca_{2-x}Na_x)$ Cu_3O_{10-y} (x=0, 0.25, 0.5) samples suppresses with Na-doping in the final compound. Sodium doped sample with a concentration of x=0, 0.25, 0.5 in CuTl 1223 samples show the onset of superconductivity at temperatures of 106.6, 108, and 109K, respectively, and the critical temperature for zero resistance at 101, 96.5 and 99.7K. The c-axis length increases and the volume of the final compound unit decreases with Na-doping. The planar oxygen mode of CuO_2 at 580 cm^{-1} and the apical oxygen modes Cu(1)-O_A-Cu (2) & Tl-O_A-Cu (2) are softened in FTIR absorption measurements indicating intrinsic incorporation of Na in the final compound. The softening of these phonon modes is related to the change in the dipole moment of the Na-doped sample. In the excess conductivity analyses the values of the coherence length along the c axis, the interlayer coupling J, the Fermi velocity V_F and the relaxation time of the carrier phase are not significantly changed by Na-doping in the final junction. Furthermore, the value of $B_{c0}(T)$, $B_{c1}(T)$ and $J_c(0)$ of the Na-doped sample did not change significantly, indicating that the number of intentional defects did not change significantly. Therefore, there is little difference between London penetration depth and Ginzburg-Landau (GL) parameters in Na-doped samples. Despite change in the X-ray diffraction spectra, a softening of phonon modes and the suppression of the zero-resistivity critical temperature, the unaltered intrinsic superconductivity parameters indicated that the role of the phase coherence of the carriers in the various CuO_2 planes is pivotal in the mechanism of superconductivity.

References:

[1] M. Mumtaz et al., "*Infield superconductivity of carbon nanotubes Cu0.5Tl0.5Ba2Ca2Cu3O10−δ superconductor composites*," AIP Advances, vol. 5, no. 10, p. 107148, Oct. 2015, doi: 10.1063/1.4935191.

[2] N. A. Khan and M. Mumtaz, "*A new $Cu_{0.5}Tl_{0.5}Ba_2Ca_2Cu_{3-y}Zn_yO_{10-\delta}$high-temperature superconductor with three ZnO2planes,"* Superconductor Science and Technology, vol. 19, no. 8, pp. 762–766, Jun. 2006, doi: 10.1088/0953-2048/19/8/012.

[3] M. Rekaby, N. H. Mohammed, M. Ahmed, and A. I. Abou-Aly, *"Synthesis, microstructure and indentation Vickers hardness for (Y_3Fe5O_{12}) x/$Cu_{0.5}Tl_{0.5}Ba_2Ca_2Cu_3O_{10-\delta}$ composites*," Applied Physics A, vol. 128, no. 4, Mar. 2022, doi: 10.1007/s00339-022-05394-3.

[4] A. Bedoya, "*SUPERCONDUCTIVITY IN COMPOSITE MATERIALS AUTHOR,"* www.academia.edu, Accessed: Sep. 01, 2022. [Online]. Available: https://www.academia.edu/16308860/SUPERCONDUCTIVITY_IN_COMPOSITE_MATERIALS_AUTHO

[**[5]** A. I. Larkin and A. A. Varlamov, "*Fluctuation Phenomena in Superconductors*," arXiv: condmat/0109177, Sep. 2001, Accessed: Aug. 31, 2022. [Online]. Available: https://arxiv.org/abs/condmat/0109177

[6] L. Essaleh, S. M. Wasim, G. Marín, C. Rincón, S. Amhil, and J. Galibert, "*Mott type variable range hopping conduction and magnetoresistance in p-type CuIn3Te5 semiconductor compound*," Journal of Applied Physics, vol. 122, no. 1, p. 015702, Jul. 2017, doi: 10.1063/1.4991004.

[7] L. G. Aslamasov and A. I. Larkin, "*The influence of fluctuation pairing of electrons on the conductivity of normal metal,"* Physics Letters A, vol. 26, no. 6, pp. 238–239, Feb. 1968, doi: 10.1016/0375-9601(68)90623-3.

[8] A. L. Solovjov, H.-U. Habermeier, and T. Haage, "*Fluctuation conductivity in YBa2Cu3O7−y films with different oxygen content. II. YBCO films with Tc≈80 K*," Low Temperature Physics, vol. 28, no. 2, pp. 99–108, Feb. 2002, doi: 10.1063/1.1461921.